2.6. Animals

Male ddY mice (5 weeks old, 25–27 g) were purchased from Shizuoka Agricultural Co-operative Association for Laboratory Animals, Shizuoka, Japan. For preparation of the tumor-bearing model, male CDF1 mice (4 weeks old) were purchased from the company mentioned above, and 1×10^6 cells of colon 26 were subcutaneously inoculated into the back of CDF1 mice. Then the mice were kept until the tumor had reached about 100 mm^3 in volume. Tumor volume is calculated as follows: volume $= 1/2 \times LW^2$ (L is the long diameter and W is the short diameter of a tumor). Animals were maintained under conventional housing conditions. All experiments with animals were performed according to the Guidelines for Animal Experimentation at Kyoto University.

2.7. Biodistribution experiments

The biodistribution experiments in both normal and tumor-bearing mice were performed according to the following method. ^{111}In-labeled dendrimer was dissolved in saline, and the concentration of dendrimer was adjusted by addition of non-radiolabeled dendrimer to the solution. The ^{111}In-labeled dendrimer solution was administrated intravenously via the tail at a dose of 1 mg/kg. At an appropriate time after the intravenous injection, blood was collected from the vena cava under ether anesthesia and the mice were sacrificed. The liver, kidneys, spleen, heart, and lungs were removed, rinsed with saline, blotted dry, and weighed. The collected blood was centrifuged for 5 min at 2000 $\times g$ to prepare a plasma sample. The collected organs and 100 μl of plasma were transferred into a counting tube, and the radioactivity of each sample was measured using a gamma counter.

For the biodistribution experiments, in which the effect of multiple injections of PEGylated KG6 on the biodistribution characteristics of the second dose was investigated, the first dose was injected 5 days before the second dose, because it has been reported that the ABC phenomenon occurred most effectively at 5 days post-injection of the first dose [20]. In this experiment, non-radiolabeled intact KG6 and PEG(76)-KG6 were used as the first dose at a concentration of 0.1 mg dendrimer/kg and 1 mg dendrimer/kg. Then, 1 mg dendrimer/kg of PEG(76)-KG6 including the radiolabeled one was administered to mice via the tail vein at 5 days after the first dose. All
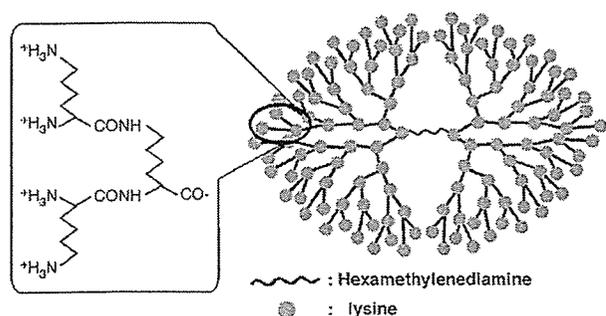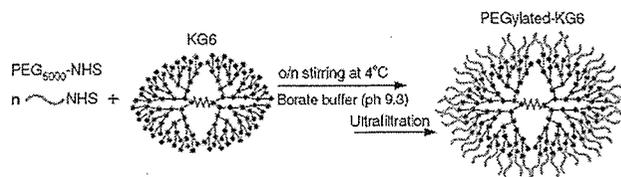

Scheme 1. Schematic presentation of the procedure used to synthesize PEGylated KG6.

subsequent procedures were performed according to the method described above.

2.8. Statistical analysis

Statistic analysis was performed using Student's paired t-test for two groups. Multiple comparisons among different generations were made with the Tukey–Kramer test. $P < 0.05$ was considered to be indicative of statistical significance.

3. Results

3.1. Synthesis of PEGylated KG6

The structure of the sixth generation lysine dendrimer (KG6) is shown in Fig. 1. In accordance with a method described previously, KG6 was synthesized using the hexamethylenediamine as the initiator core. The coupling and de-protection steps were performed with a yield of about 75–98%. In the next step, KG6 was reacted with an equivalent molar ratio of DTPA anhydride. Then, PEGylated KG6 was synthesized according to Scheme 1. The PEGylation was performed at two different molar ratios. As a result of quantification of the introduced PEG chain by the barium–iodine method [17], two PEGylated KG6 derivatives having different modification rates have been synthesized. The numbers of introduced PEG chains were 10 and 76.1 per KG6 molecule (Table 1). We call these derivatives PEG(10)-KG6 and PEG(76)-KG6, respectively.

3.2. Physicochemical properties of PEGylated KG6 derivatives

The physicochemical properties of PEGylated KG6 derivatives were analyzed by Zetasizer Nano ZS (Table 1). The mean diameter of PEG(10)-KG6 was slightly larger (about 7.75 nm) than that of intact KG6 (about 5.85 nm), while the particle size

Fig. 1. Structure of the sixth generation dendritic poly(L-lysine) (KG6).

Table 1
Physicochemical properties of PEGylated KG6 in PBS

	No. of PEG$_{5000}$[a]	No. of –NH$_2$ groups[b]	Particle size (nm)	Zeta-potential (mV)
KG6	0	128	5.85±0.06	19.77±0.30
PEG(10)-KG6	10	118	7.75±0.70	0.00±0.03
PEG(76)-KG6	76.2	51.8	16.92±0.13	−6.51±0.18

Each value represents the mean±SD of three experiments.
[a] The number of PEG$_{5000}$ was determined by the barium–iodine method.
[b] The number of surface amino groups was determined by subtracting the result of the barium–iodine method from the number of native KG6's surface amino groups.

of PEG(76)-KG6 was much larger (about 16.9 nm). Although the zeta-potential of intact KG6 was positive, both PEGylated derivatives had an almost neutral zeta-potential.

3.3. Plasma concentration of ^{111}In-labeled PEGylated KG6 derivatives

Fig. 2 shows the short-term (A) and long-term (B) plasma concentration profiles of ^{111}In-labeled PEGylated KG6 derivatives after intravenous injection into mice. Although the intact KG6 was rapidly eliminated from the circulation within a few minutes, the retention of PEGylated KG6 derivatives was enhanced by modification with PEG chains (Fig. 2A). This enhancing effect was acquired even by introducing ten PEG chains. However, as the modification rate increased, so too did the amount of PEGylated KG6 retained in the blood stream. In the case of PEG(76)-KG6, about 20% of the injected dose was still circulating in the blood stream (Fig. 2B).

3.4. Tissue distribution of ^{111}In-labeled PEGylated KG6 derivatives

The biodistribution characteristics of PEGylated KG6 derivatives and intact KG6 were evaluated until 60 min post-intravenous injection into mice by measuring the radioactivity in the organs and urine. The dendrimers were almost undetectable in the spleen, heart, lung, and urine (data not shown).
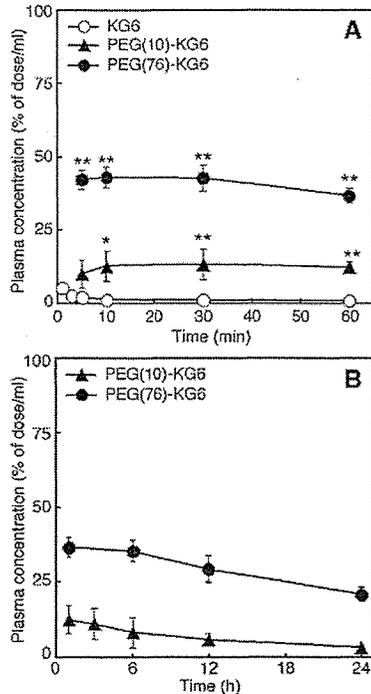

Fig. 2. The short-term (A) and long-term (B) plasma concentration profiles of ^{111}In-labeled PEGylated KG6 after intravenous administration to mice at a dose of 1 mg/kg. Each value represents the mean ± SD of three experiments. The intact KG6 (O), PEG(10)-KG6 (▲), and PEG(76)-KG6 (●) were subjected to biodistribution experiments. Statistically significant differences (*, $P<0.05$; **, $P<0.01$) between PEGylated KG6 and intact KG6 at each time point.
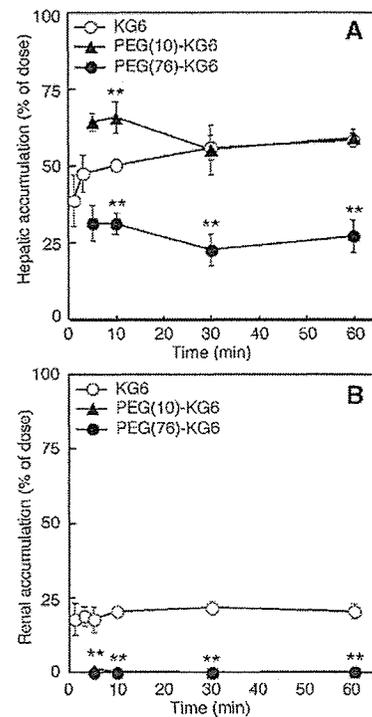

Fig. 3. Hepatic (A) and renal (B) accumulation of ^{111}In-labeled PEGylated KG6 after intravenous administration to mice at a dose of 1 mg/kg. The intact KG6 (O), PEG(10)-KG6 (▲), and PEG(76)-KG6 (●) were subjected to biodistribution experiments. Each value represents the mean ± SD of three experiments. Statistically significant differences (*, $P<0.05$; **, $P<0.01$) between PEGylated KG6 and intact KG6 at each time point.

The amount of PEG(10)-KG6 accumulated in the liver was the almost same as that of intact KG6 (Fig. 3A). In contrast, the accumulation of PEG(76)-KG6 in liver was fairly suppressed (Fig. 3A). On the other hand, the renal accumulation of intact KG6 was observed, whereas no detectable levels of radioactivity derived from PEGylated KG6 derivatives were detected from the kidneys (Fig. 3B).

3.5. Tumor accumulation of PEG(76)-KG6 in the tumor-bearing model mice

In order to clarify whether the intravenously injected PEGylated KG6 accumulated into the solid tumor tissue or not, a biodistribution analysis of PEG(76)-KG6 which showed a more advantageous blood retention was performed in tumor-bearing mice (Fig. 4). In the case of intact KG6, no significant accumulation was observed in the tumor at any time point. In contrast, PEG(76)-KG6 gradually accumulated into the tumor. The tumor accumulation rate of PEG(76)-KG6 reached 14.6% of dose/g tumor, whereas that of intact KG6 was only 2.2% of dose/g tumor even at 24 h post-injection.

3.6. Plasma concentration of ^{111}In-labeled PEGylated KG6 after multiple injections

In order to confirm whether the first dose of dendrimers (intact or PEGylated KG6) affect the biodistribution characteristics of the
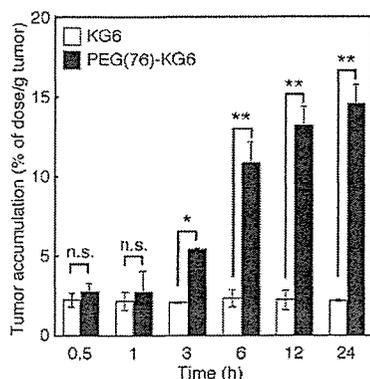
Fig. 4. Time-dependent tumor accumulation of ^{111}In-labeled PEG(76)-KG6 after intravenous administration to CT26 tumor-bearing CDF1 mice at a dose of 1 mg/kg. Each value represents the mean±SD of three experiments. Closed and open bars represent tumor accumulation of PEG(76)-KG6 and intact KG6, respectively. Statistically significant differences (*, $P<0.05$; **, $P<0.01$) between PEG(76)-KG6 and intact KG6 at each time point.

second dose of PEG(76)-KG6, pre-injection of the dendrimers was performed at 5 days before the biodistribution analysis of the second dose of PEG(76)-KG6. We used 0.1 mg/kg and 1 mg/kg of intact KG6 or PEG(76)-KG6 as the first dose of dendrimers. In addition, we used saline treatment as a control. The blood concentration profiles of the second dose of intravenously administered PEG(76)-KG6 are shown in Fig. 5. As shown in Fig. 5A and B, no significant changes in blood concentration
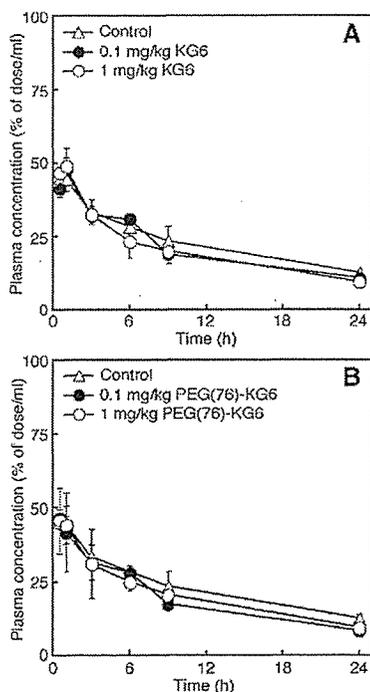

Fig. 5. Plasma concentration profiles of ^{111}In-labeled PEG(76)-KG6 after intravenous administration in intact KG6 (A) or PEG(76)-KG6 (B) pretreated mice. Each value represents the mean±SD of three experiments. The mice were pretreated with intact KG6 or PEG(76)-KG6 at a concentration of 0.1 mg/kg (●) and 1 mg/kg (O). The saline pretreatment was used as a control (△). Subsequently, ^{111}In-labeled PEG(76)-KG6 was intravenously administered at day 5 post-first injection.
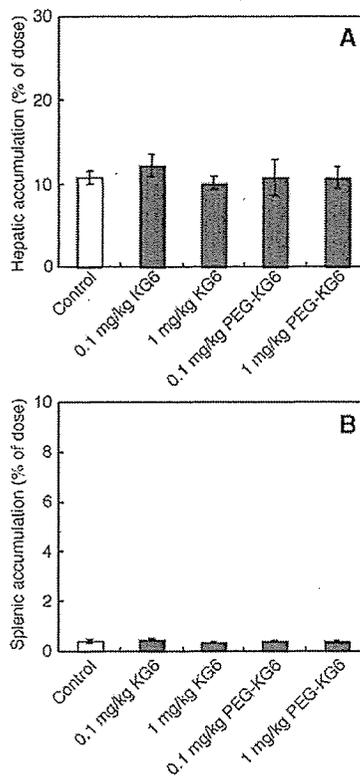

Fig. 6. Hepatic (A) and splenic (B) accumulation of ^{111}In-labeled PEG(76)-KG6 in intact KG6 or PEG(76)-KG6 pretreated mice at 24 h post-injection. The saline pretreatment was used as a control. Each value represents the mean±SD of three experiments.

profiles of the second dose of PEG(76)-KG6 were observed even if the concentration and formulation of the first dose were different.

3.7. Hepatic and splenic accumulation of ^{111}In-labeled PEGylated KG6

Since the organs of the reticuloendothelial system (RES), such as the liver and spleen, play an important role in the metabolism and excretion of foreign substance, we evaluated the hepatic and splenic accumulation of the second dose of PEG (76)-KG6 at 24 h post-injection (Fig. 6). Both the hepatic and splenic accumulation rate were almost the same under all conditions used, though we administered two types of dendrimers at two different concentrations as the first dose.

4. Discussion

It is expected that a more functional and safer drug carrier system will be developed. We have previously reported that KG6 showed no significant toxicity to cultured cells compared with the PAMAM dendrimer [12]. More recently, we have also reported that KG6 has no acute hepatic toxicity and the PEGylation of KG6 caused a sustained retention of KG6 in the blood stream [14]. Therefore, in this study, we employed KG6 as a candidate base molecule for a tumor-targeting drug carrier that is highly safe, and

evaluated the physicochemical properties and biodistribution characteristics of intact and PEGylated KG6.

The synthesis of lysine dendrimers up to the sixth generation could be achieved with good yields, and then, the PEGylation of KG6 was performed in accordance with the method described in Scheme 1. As a result of the quantification of the PEGylation rate, two PEGylated KG6 derivatives the modification rate of which is about 7.8% (PEG(10)-KG6) and 59.4% (PEG(76)-KG6), respectively, were synthesized (Table 1). The particle size of intact KG6 was about 5.85 nm, whereas that of PEG(10)-KG and PEG(76)-KG6 was about 7.75 nm and 16.92 nm, respectively (Table 1). Both PEG(10)-KG6 and PEG(76)-KG6 showed almost a neutral zeta-potential, while the zeta-potential of intact KG6 was positive (Table 1). These increments in size and changes of zeta-potential from positive to neutral suggest that PEGylation of KG6 was certainly achieved. Since the polymeric micelles and liposomes are assemblies of many molecules, the reproducibility may be low. The hyperbranched polymers that have many branches like dendrimers are not assemblies, but they are usually a mixture of many polymer molecules with irregular structure and size. Hence, the reproducibility of this type of polymer may be also not good. The linear poly-L-lysines also consist of lysines. However, almost of all commercially available linear poly-L-lysine is a mixture of molecules with various molecular weight due to their synthetic procedure. Though linear poly-L-lysine can be synthesized as uniform molecules by solid phase synthesis, mass production is very difficult. In contrast to these compounds, the lysine dendrimer can be mass-produced as a monodispersed molecule not an assembly; accordingly its reproducibility would be better than that of polymeric micelles, liposomes and hyperbranched polymers. In addition, dendrimers are smaller in size than polymeric micelles and liposomes. Therefore the use of dendrimers as drug carriers probably enables one to achieve a more precise and effective drug targeting.

In order to evaluate biodistribution of the characteristics of intact and PEGylated KG6, these dendrimers were radiolabeled with [^{111}In] and injected into mice. Intravenously administered intact KG6 was rapidly eliminated from the circulation within few minutes (Fig. 2A). This rapid elimination is probably due to accumulation in the liver and kidney in the early phase (Fig. 3). However, PEGylation of KG6 enhances the retention in blood, and this effect is boosted as the PEGylation rate is increased (Fig. 2A). However, PEG(10)-KG6 accumulated in the liver at almost the same level as intact KG6, whereas the hepatic accumulation of PEG(76)-KG6 was slightly suppressed (Fig. 3A). In addition, PEGylation of KG6 resulted in no renal accumulation (Fig. 3B). As these results show, the non-specific interaction with biomolecules and non-specific accumulation in organs via electrostatic interaction is suppressed by modification with PEG chains. Consequently, the retention of PEGylated KG6 derivatives in the blood stream was enhanced.

To investigate whether the PEGylated KG6 shows tumor tissue accumulativeness, PEG(76)-KG6, which showed a better blood retention, was radiolabeled and was also subjected to tumor-bearing mice. As shown in Fig. 4, although the intact KG6 hardly showed tumor accumulativeness, PEG(76)-KG6

gradually and effectively accumulated in tumor tissue. Maeda and Matsumura reported that macromolecules ~200 nm in size and with a prolonged retention in blood extravasate into the interstitial space of solid tumors through the poorly constructed tumoral vascular wall and stay there because tumors usually lack effective lymphatic drainage; consequently, they accumulate in tumor tissue effectively by the EPR effect [21]. Since PEG(76)-KG6 fulfills the requirement of blood retention and size for causing the EPR effect (Table 1 and Fig. 2), PEG(76)-KG6 probably accumulated in the tumor tissue via this effect. This result is well consistent with that of polymeric micelles having a PEG moiety and PEGylated liposomes [22–26]. These results suggest that PEGylation is applicable to dendrimeric molecules like lysine dendrimers for tumor targeting.

As far as the actual clinical use of drug formulations is concerned, multiple administrations are frequently performed. It has been reported that multiple injections of PEGylated liposomes induce an accelerated blood clearance (ABC) phenomenon on the second injection [27]. Therefore, the induction of the ABC phenomenon may be an obstacle to therapy. Hence, we evaluated the effect of multiple administrations on the biodistribution characteristics of the second dose of PEGylated KG6. As shown in Fig. 5, the blood concentration profile of the second dose of PEG(76)-KG6 was unchanged regardless of the composition and concentration of pre-injected dendrimers. Moreover, in the case of PEGylated liposomes, it has been reported that the ABC phenomenon was probably due to uptake by the reticuloendothelial system (RES) particularly in the liver [28]. However, no significant increase in hepatic or splenic accumulation was observed under any conditions we tested (Fig. 6). These results suggest that PEGylated KG6 would become a multi-administrable drug carrier molecule.

The following two methods would be available for drug loading to PEGylated lysine dendrimer: 1) covalent bonding via surface primary amine groups, 2) non-covalent drug incorporation into the inner space of lysine dendrimer taking advantage of the physicochemical interaction such as hydrophobic interaction. In the case of covalent bonding, the drugs would be stably bonded to the dendrimer, but the drugs must have functional group to form a covalent bond with primary amino groups of lysine dendrimer and the appropriate device to release the drugs at target site may be needed. Furthermore, it is necessary to consider the loss of amino groups by conjugation of PEG chains and the steric hindrance of introduced PEG chains. In contrast, in the case of non-covalent incorporation of drugs, no peculiar functional groups or devices are required. In this case, however, the alteration of inner structure of dendrimer may be needed to hold the drugs stably. Moreover, the size and structural feature would be restricted because the inner space of lysine dendrimer is limited. Probably, about up to 1000 in molecular weight is acceptable and the planar structure such as anti-cancer drugs is suitable. Although the appropriate drug loading method should be selected, the non-covalent incorporation would be more suitable as a drug loading method for PEGylated lysine dendrimer.

In conclusion, we synthesized KG6 and two PEGylated derivatives thereof and evaluated their biodistribution characteristics

in mice and tumor accumulativeness in tumor-bearing mice. In addition, we confirmed that multiple injections affect the biodistribution characteristics of the second dose of PEGylated KG6. The unfavorable biodistribution properties of intact KG6, such as rapid elimination from the blood and non-specific uptake by the liver and kidney, could be improved by modification with PEG chains. In addition, PEG(76)-KG6 was significantly accumulated in tumor via the EPR effect, whereas the intact KG6 showed no significant accumulation. Moreover, compared with a single administration, the biodistribution characteristics of the second dose of PEGylated KG6 showed no change on multiple injections. These results suggest the PEGylated lysine dendrimers to be useful as a base material for a clinically applicable tumor-targeting drug carrier.

Acknowledgements

References

[1] N.D. James, R.J. Coker, D. Tomlinson, J.R. Harris, M. Gompels, A.J. Pinching, J.S. Stewart, Liposomal doxorubicin (Doxil): an effective new treatment for Kaposi's sarcoma in AIDS, Clin. Oncol. (R. Coll. Radiol.) 6 (1994) 294–296.

[2] D.S. Alberts, D.J. Garcia, Safety aspects of pegylated liposomal doxorubicin in patients with cancer, Drugs 54 (1997) 30–35.

[3] R. Esfand, D.A. Tomalia, Poly(amidoamine) (PAMAM) dendrimers: from biomimicry to drug delivery and biomedical applications, Drug Discov. Today 6 (2001) 427–436.

[4] S.E. Stiriba, H. Frey, R. Haag, Dendritic polymers in biomedical applications: from potential to clinical use in diagnostics and therapy, Angew. Chem., Int. Ed. 41 (2002) 1329–1334.

[5] J.F. Kukowska-Latallo, K.A. Candido, Z. Cao, S.S. Nigavekar, I.J. Majoros, T.P. Thomas, L.P. Balogh, M.K. Kahn, J.R. Baker Jr., Nanoparticle targeting of anticancer drug improves therapeutic response in animal model of human epithelial cancer, Cancer Res. 65 (2005) 5317–5324.

[6] H. Yoo, R.L. Juliano, Enhanced delivery of antisense oligonucleotides with fluorophore-conjugated PAMAM dendrimers, Nucleic Acids Res. 28 (2000) 4225–4231.

[7] J.S. Choi, K. Nam, J.Y. Park, J.B. Kim, J.K. Lee, J.S. Park, Enhanced transfection efficiency of PAMAM dendrimer by surface modification with L-arginine, J. Control. Release 99 (2004) 445–456.

[8] K. Wada, H. Arima, T. Tsutsumi, F. Hirayama, K. Uekama, Enhancing effects of galactosylated dendrimer/alpha-cyclodextrin conjugates on gene transfer efficiency, Biol. Pharm. Bull. 28 (2005) 500–505.

[9] H. Kobayashi, S. Kawamoto, R.A. Star, T.A. Waldmann, Y. Tagaya, M.W. Brechbiel, Micro-magnetic resonance lymphangiography in mice using a novel dendrimer-based magnetic resonance imaging contrast agent, Cancer Res. 63 (2003) 271–276.

[10] H. Kobayashi, S.K. Jo, S. Kawamoto, H. Yasuda, X. Hu, M.V. Knopp, M.W. Brechbiel, P.L. Choyke, R.A. Star, Polyamine dendrimer-based MRI contrast agents for functional kidney imaging to diagnose acute renal failure, J. Magn. Reson. Imaging 20 (2004) 512–518.

[11] N. Malik, R. Wiwattanapatapee, R. Klopsch, K. Lorenz, H. Frey, J.W. Weener, E.W. Meijer, W. Paulus, R. Duncan, Dendrimers: relationship between structure and biocompatibility in vitro, and preliminary studies on the biodistribution of ^{125}I-labelled polyamidoamine dendrimers in vivo, J. Control. Release 65 (2000) 133–148.

[12] M. Ohsaki, T. Okuda, A. Wada, T. Hirayama, T. Niidome, H. Aoyagi, In vitro gene transfection using dendritic poly(L-lysine), Bioconjug. Chem. 13 (2002) 510–517.

[13] T. Okuda, A. Sugiyama, T. Niidome, H. Aoyagi, Characters of dendritic poly(L-lysine) analogues with the terminal lysines replaced with arginines and histidines as gene carriers in vitro, Biomaterials 25 (2004) 537–544.

[14] T. Okuda, S. Kawakami, T. Maeie, T. Niidome, F. Yamashita, M. Hashida, Biodistribution characteristics of amino acid dendrimers and their PEGylated derivatives after intravenous administration, J. Control. Release 114 (2006) 69–77.

[15] C.G. Fields, D.H. Lloyd, R.L. Macdonald, K.M. Otteson, R.L. Noble, HBTU activation for automated Fmoc solid phase peptide synthesis, Pept. Res. 4 (1991) 95–101.

[16] D. Hnatowich, W.W. Layne, R.L. Childs, The preparation and labeling of DTPA-coupled albumin, J. Appl. Radiat. Isot. 12 (1982) 327–332.

[17] B. Skoog, Determination of polyethylene glycols 4000 and 6000 in plasma protein preparations, Vox Sang. 37 (1979) 345–349.

[18] J.R. Duncan, M.J. Welch, Intracellular metabolilsm of indium-111-DTPA-labeled receptor targeted proteins, J. Nucl. Med. 34 (1993) 1728–1738.

[19] F. Staud, M. Nishikawa, K. Morimoto, Y. Takakura, M. Hashida, Disposition of radioactivity after injection of liver-targeted proteins labeled with ^{111}In or ^{125}I. Effect of labeling on distribution and excretion of radioactivity in rats, J. Pharm. Sci. 88 (1999) 577–585.

[20] T. Ishida, M. Harada, X.Y. Wang, M. Ichihara, K. Irimura, H. Kiwada, Accelerated blood clearance of PEGylated liposomes following preceding liposome injection: effects of lipid dose and PEG surface-density and chain length of the first-dose liposomes, J. Control. Release 105 (2005) 305–317.

[21] Y. Matsumura, H. Maeda, A new concept for macromolecular therapeutics in cancer chemotherapy: mechanism of tumoritropic accumulation of proteins and the antitumor agent smancs, Cancer Res. 46 (1986) 6387–6392.

[22] T. Nakanishi, S. Fukushima, K. Okamoto, M. Suzuki, Y. Matsumura, M. Yokoyama, T. Okano, Y. Sakurai, K. Kataoka, Development of the polymer micelle carrier system for doxorubicin, J. Control. Release 74 (2001) 295–302.

[23] A.N. Lukyanov, W.C. Heartner, V.P. Torchilin, Increased accumulation of PEG-PE micelles in the area of experimental myocardial infarction in rabbits, J. Control. Release 97 (2004) 187–193.

[24] Y. Bae, N. Nakanishi, S. Fukushima, H. Koyama, M. Yasuhiro, K. Kataoka, Preparation and biological characterization of polymeric micelle drug carriers with intracellular pH-triggered drug release properties: tumor permeability, controlled subcellular drug distribution, and enhanced in vivo antitumor efficacy, Bioconjug. Chem. 16 (2005) 122–130.

[25] O. Ishida, K. Maruyama, H. Tanahashi, M. Iwatsuru, K. Sasaki, M. Eriguchi, H. Yanagie, Liposomes bearing polyethyleneglycol-coupled transferrin with intracellular targeting property to the solid tumor in vivo, Pharm. Res. 18 (2001) 1042–1048.

[26] Y. Matsumura, M. Gotoh, K. Muro, Y. Yamada, K. Shirao, Y. Shimada, M. Okuwa, S. Matsumoto, Y. Miyata, H. Ohkura, K. Chin, S. Baba, T. Yamao, A. Kannami, Y. Takamatsu, K. Ito, K. Takahashi, Phase I and phamacokinetic study of MCC-465, a doxorubicin (DXR) encapsulated in PEG immunoliposome, in patients with metastatic stomach cancer, Ann. Oncol. 15 (2004) 517–525.

[27] E.T. Dams, P. Laverman, W.J. Oyen, G. Storm, G.L. Scherphof, J.W. van Der Meer, F.H. Corstens, O.C. Boerman, Accelerated blood clearance and altered biodistribution of repeated injections of sterically stabilized liposomes, J. Pharmacol. Exp. Ther. 292 (2000) 1071–1079.

[28] T. Ishida, T. Ichikawa, M. Ichihara, Y. Sadzuka, H. Kiwada, Effect of the physicochemical properties of initially injected liposomes on the clearance of subsequently injected PEGylated liposomes in mice, J. Control. Release 95 (2004) 403–412.

Intracellular Trafficking Is the Important Process That Determines the Optimal Charge Ratio on Transfection by Galactosylated Lipoplex in HepG2 Cells

Yasunori Saito, Shigeru Kawakami, Yoshiyuki Yabe, Fumiyoshi Yamashita, and Mitsuru Hashida*

Department of Drug Delivery Research, Graduate School of Pharmaceutical Sciences, Kyoto University; Sakyo-ku, Kyoto 606–8501, Japan. Received May 23, 2006; accepted June 22, 2006; published online June 26, 2006

The purpose of the present study was to gain insight into the major factors affecting transfection efficiency with galactosylated lipoplex in HepG2 cells. In this study, lipoplex and galactosylated lipoplex were examined at different charge ratios (− : +): 1.0 : 1.2, 1.0 : 2.3, 1.0 : 3.1, 1.0 : 4.7, and 1.0 : 7.0. The particle size and zeta potential of the both lipoplexes was dependent on the charge ratio. Cellular uptake was evaluated by using [^{32}P]-labeled pCMV-Luc and this showed that the cellular uptake of galactosylated lipoplex was significantly higher than that of lipoplex at a charge ratio ranging from 1.0 : 2.3 to 1.0 : 7.0. As the charge ratio increased in both lipoplexes, the apparent cellular uptake increased. Transfection activity by galactosylated lipoplex was significantly higher than that by lipoplex except at a charge ratio of 1.0 : 7.0. The optimal charge ratio for transfection efficacy was 1.0 : 2.3 and transfection was reduced at higher charge ratios. Both lipoplexes exhibited no significant cytotoxicity at any charge ratio. In conclusion, it is suggested that intracellular trafficking, rather than the degree of uptake and cytotoxicity, is the important process that determines the optimal charge ratio of galactosylated lipoplex in HepG2 cells.

Key words   gene delivery; hepatocytes; targeting; liposome; lipoplex

Non-viral vectors have advantages in terms of their simplicity of use and ability to be produced on a large scale if necessary. Among various types of non-viral vectors, cationic liposome-mediated gene transfection is one of the most promising approaches due to the high transfection efficiency.[1—4] Gene delivery to hepatocytes is of great therapeutic potential, since the cells are responsible for the synthesis of a wide variety of proteins that play important biological roles both inside and outside the liver. To achieve targeted gene delivery to hepatocytes, galactose has been shown to be a promising targeting ligand because these cells possess a large number of asialoglycoprotein receptors that recognize the galactose units on the synthetic galactosylated carriers.[5—7] Recently, we have developed galactosylated cationic liposomes containing cholesten-5-yloxy-*N*-(4-((1-imino-2-D-thiogalactosylethyl)amino)butyl)formamide (Gal-C4-Chol) for hepatocyte-selective gene transfection *via* asialoglycoprotein receptor-mediated endocytosis after intraportal administration into mice.[8—10] In this approach, plasmid DNA is mixed with preformed galactosylated cationic liposomes to form galactosylated lipoplex, based on electrostatic interaction, which can then interact with hepatocytes and be taken up by them. Since Gal-C4-Chol possesses an imino group for binding to plasmid DNA *via* electrostatic interaction, many galactose units can be introduced on the liposomal surface without loss of binding affinity to plasmid DNA. These promising properties of our galactosylated lipoplex enable hepatocyte-selective gene transfer to be achieved under *in vivo* conditions. The overall ratio of the positive charge on a cationic lipid to the negative charge on a plasmid DNA seems to be a critical determinant of this phenomenon. It is generally accepted that the physicochemical characteristics of the galactosylated lipoplex prepared at different mixing ratios are so different that their cellular uptake, subsequent intracellular trafficking and resultant transfection efficiency

would be significantly affected. However, there is little published information on the relationship between these physico-chemical and biological factors in the lipoplex and/or galactosylated lipoplex.

Previously, we have investigated the effect of the pDNA-*N*-[1-(2,3-dioleyloxy)propyl]-*N*,*N*,*N*-trimethylammonium chloride (DOTMA)/dioleoylphosphatidylethanolamine (DOPE) liposomes mixing (charge) ratio on the particle size, zeta potential and structure of the lipoplex, which directly affects cellular uptake, intracellular distribution of the complex, and the subsequent gene expression efficiency. And we have demonstrated that the mixing (charge) ratio of plasmid DNA complexed with DOTMA/DOPE liposomes significantly affects the intracellular trafficking, which is an important determinant of the optimal charge ratio in cationic liposome-mediated transfection.[11] The *in vivo* gene transfection efficacy by lipoplex was markedly affected by the type of neutral lipid. Previously, we have demonstrated that the transfection efficacy of cholesterol containing galactosylated cationic liposomes (DOTMA/cholesterol/Gal-C4-Chol) in hepatocytes was markedly higher than that of DOPE, which is a pH-sensitive lipid,[12] containing galactosylated cationic liposomes (DOPE/Gal-C4-Chol) after intraportal administration.[8] In order to achieve a more efficient gene carrier system, the limiting processes for gene expression needed to be investigated. However, the relationships involved in cholesterol-containing galactosylated cationic liposome-mediated gene transfer, cellular binding and uptake and intracellular trafficking are not yet fully understood.

In the present study, transfection efficiencies of galactosylated lipoplex were evaluated using cultured cells in relation to their physicochemical properties. Then, the cellular uptake, intracellular trafficking and cytotoxicity of galactosylated lipoplex were also examined in human hepatoma HepG2 cells, which are known to express asialoglycoprotein

receptors. It is suggested that intracellular trafficking, rather than the degree of uptake and cytotoxicity, is the important process that determines the optimal charge ratio of galactosylated lipoplex in HepG2 cells. pCMV-Luc was selected as a model plasmid DNA for evaluating the gene expression by luciferase. DOTMA/cholesterol liposomes and DOTMA/cholesterol/Gal-C4-Chol liposomes were selected as control cationic liposomes and galactosylated cationic liposomes, respectively.

MATERIALS AND METHODS

Materials N-(4-Aminobutyl) carbamic acid *tert*-butyl ester and DOTMA were obtained from Tokyo Kasei Kogyo Co., Ltd. (Tokyo, Japan). Cholesterol was obtained from Nacalai Tesque, Inc. (Kyoto, Japan). Cholesterol test-E Wako was purchased from Wako Pure Chemical Industries, Ltd. (Osaka, Japan). Cholesteryl chloroformate was obtained from Sigma Chemicals, Inc. (St. Louis, MO, U.S.A.). Dulbecco's modified Eagle's minimum essential medium (DMEM). Fetal bovine serum (FBS) was obtained from Biowhittaker (Walkersville, MD, U.S.A.). Opti-MEM I® and other culture reagents were obtained from Gibco BRL (Grand Island, NY, U.S.A.). All other chemicals were of the highest purity available.

Construction and Preparation of Plasmid DNA (pCMV-Luc) pCMV-Luc was constructed by subcloning the *Hin*dIII/*Xba*I firefly luciferase cDNA fragment from pGL3-control vector (Promega Co., Madison, WI, U.S.A.) into the polylinker of pcDNA3 vector (Invitrogen, Carlsbad, CA, U.S.A.). Plasmid DNA was amplified in the *Escherichia coli* strain DH5a, isolated, and purified using a QIAGEN Endofree Plasmid Giga Kit (QIAGEN GmbH, Hilden, Germany). Purity was confirmed by 1% agarose gel electrophoresis followed by ethidium bromide staining and the plasmid DNA concentration was measured by UV absorption at 260 nm.

Synthesis of Gal-C4-Chol Gal-C4-Chol was synthesized as reported previously.[13] Briefly, cholesteryl chloroformate and N-(4-aminobutyl)carbamic acid *tert*-butyl ester were reacted in chloroform for 24 h at room temperature. A solution of trifluoroacetic acid and chloroform was added dropwise and the mixture was stirred for 4 h at 4 °C. The solvent was evaporated to obtain N-(4-aminobutyl)-(cholesten-5-yloxyl)formamide which was then combined with 2-imino-2-methoxyethyl-1-thiogalactoside and the mixture was stirred for 24 h at 37 °C. After evaporation, the resultant material was suspended in water, dialyzed against distilled water for 48 h (12 kDa cut-off dialysis tubing), and then lyophilized.

Preparation of Galactosylated Cationic Liposomes Galactosylated cationic liposomes were prepared as reported previously.[8,10] The mixtures of DOTMA, cholesterol, and Gal-C4-Chol were dissolved in chloroform at a molar ratio of 2 : 1 : 1 for galactosylated cationic liposomes, vacuum-desiccated, and resuspended in sterile 5% dextrose solution at a concentration of 1 mg total lipids per ml. The suspension was sonicated for 3 min and the resulting liposomes were extruded 5-times through 0.45 μm polycarbonate membrane filters. The concentration of liposomes was adjusted by measuring the cholesterol concentration using the cholesterol test-E Wako.

Preparation of Lipoplex and Galactosylated Lipoplex The lipoplex and galactosylated lipoplex were prepared as reported previously.[8,10] Briefly, pDNA in sterile 5% dextrose solution was mixed with an equal volume of (galactosylated) cationic liposomes and incubated for 30 min. The mixing ratio of liposomes and pDNA was expressed as a charge ratio, which is the molar ratio of cationic lipids to pDNA phosphate residues.[14]

Evaluation of Physicochemical Properties The lipoplex and galactosylated lipoplex were dissolved at a plasmid DNA concentration of up to 1 μg/ml, and then their particle size and zeta-potential were measured by Zetasizer Nano ZS (Malvern Instruments Ltd., U.K.).

Uptake Experiment HepG2 cells were obtained from American Type Culture Collection (Manassas, VA, U.S.A.) and maintained in DMEM supplement with 10% FBS at 37 °C under an atmosphere of 5% CO_2 in air. The cells were plated on a 6-well cluster dish at a density of 2×10^5 cells/10.5 cm^2 and cultivated in 2 ml DMEM supplement with 10% FBS. Twenty-four hours later, the culture medium was replaced with an equivalent volume of HBSS containing 1 kBq/ml [^{32}P] plasmid DNA, 1 μg/ml cold plasmid DNA and cationic liposomes. After incubation for 3 h at 4 or 37 °C for given time periods, the solution was immediately removed by aspiration, the cells were washed 5-times with ice-cold HBSS buffer and solubilized in 1 ml 0.3 N NaOH solution with 10% Triton X-100. The radioactivity was measured by liquid scintillation counting (LSC-500, Beckman, Tokyo, Japan). The radioactivity data were normalized with respect to the protein contents of the cells. The protein content was determined by a modification of the Lowry method using Protein Quantification Kit (Dojindo Molecular Technologies, Inc., Gaithersburg, MD, U.S.A.).

Transfection Experiment The HepG2 cells were plated on a 6-well cluster dish at a density of 2×10^5 cells/10.5 cm^2 and cultivated in 2 ml DMEM supplemented with 10% FBS. After 24 h, the culture medium was replaced with Opti-MEM I® containing 1 μg/ml plasmid DNA and cationic liposomes. Six hours later, the incubation medium was replaced again with DMEM supplement with 10% FBS and incubated for an additional 42 h. Then, the cells were scraped off and suspended in 200 μl pH 7.4 phosphate-buffered saline (PBS). One hundred microliters cell suspension was subjected to three cycles of freezing (liquid N_2 for 3 min) and thawing (37 °C for 3 min), followed by centrifugation at 10000 g for 3 min. The supernatants were stored at −20 °C until the luciferase assays were performed. Ten microliters supernatant was mixed with 100 μl luciferase assay buffer (Picagene, Toyo Ink, Tokyo, Japan) and the light produced was immediately measured using a luminometer (Lumat LB 9507, EG & G Berthold, Bad Wildbad, Germany). The activity is indicated as the relative light units per mg protein. The radioactivity data were normalized with respect to the protein content of the cells. The protein content of the cell suspension in PBS was determined by a modified Lowry method using Protein Quantification Kit (Dojindo Molecular Technologies, Inc., Gaithersburg, MD, U.S.A.).

Cytotoxicity Experiment Cytotoxicity was evaluated by MTT assay. The cells, plated on a 24-well plate at a density of 0.38×10^5 cells/2.0 cm^2, were incubated in 500 μl Opti-MEM I® containing 1 μg/ml plasmid DNA and cationic lipo-

somes. Six hours later, the incubation medium was replaced with DMEM supplement with 10% FBS and incubated for an additional 42 h. After addition of 0.5 mg/ml MTT solution, the solution was incubated overnight at 37 °C with 10% SDS solution. The absorbance was measured at test and reference wavelengths of 570 and 660 nm, respectively, in a two-wavelength microplate photometer (Bio-Rad Model 450, Hercules, CA, U.S.A.).

Statistical Analysis Statistical analysis was performed using Student's paired t-test for two groups and the Tukey–Kramer test for multiple comparisons between groups. $p < 0.05$ was considered to be indicative of statistical significance.

RESULTS

Physicochemical Properties of Galactosylated Lipoplex The particle size and the zeta potential of the both lipoplex and galactosylated lipoplex were examined at different charge ratios. The particle size and zeta potential of both lipoplexes depended on the charge ratio (Figs. 1, 2). The particle size was about 200 nm at a charge ratio of 1.0 : 1.2 and the particle size increased in parallel with the ratio and then decreased at higher charge ratios. The zeta potential of both the lipoplex and galactosylated lipoplex also depended on the charge ratio (Fig. 2). The zeta potential was −4 mV at a

charge ratio of 1.0 : 1.2 and became positive at a charge ratio of 1.0 : 1.6 (about+40 mV). At a charge ratio of 1.0 : 7.5, both the lipoplex and galactosylated lipoplex exhibited a positive zeta potential (about+60 mV).

Uptake Characteristics of Galactosylated Lipoplex In order to investigate a possible correlation between the cellular uptake of lipoplex and subsequent gene expression, the cellular association of the lipoplex containing ^{32}P-labeled plasmid DNA was evaluated at 4 and 37 °C at different charge ratios (Fig. 3). Cellular uptake of galactosylated lipoplex was significantly higher than that of lipoplex at a charge ratio (− : +) from 1.0 : 2.3 to 1.0 : 7.0. As the charge ratio increased in both lipoplexes, the apparent cellular association at both temperatures increased. At a charge ratio (− : +) of 1.0 : 1.2, on the other hand, the apparent cellular uptake by galactosylated lipoplex was similar to that by lipoplex.

Transfection Characteristics of Galactosylated Lipoplex HepG2 cells were selected for transfection with the lipoplex or galactosylated lipoplex prepared at different charge ratios (Fig. 4). Extremely large differences in the gene expression level were observed at different charge ratios. Transfection activity by galactosylated lipoplex was significantly higher than that by lipoplex at a charge ratio (− : +) of 1.0 : 1.2 to 1.0 : 4.7. The optimal charge ratio (− : +) for transfection efficacy in both lipoplexes was 1.0 : 2.3 and transfection was reduced at higher charge ratios. In contrast, transfection efficacy of both lipoplexes was almost identical when they were prepared at a charge ratio (− : +) of 1.0 : 7.0.

Internalization and Transfection Efficacy per Internalization amount of Galactosylated Lipoplex We roughly
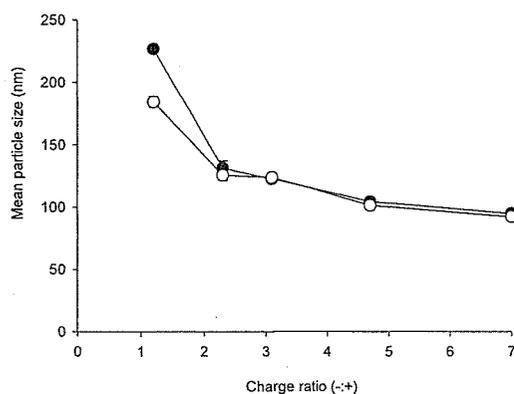

Fig. 1. The Mean Particle Size of the Lipoplex (Open Circle) and Galactosylated Lipoplex (Closed Circle) at Different Charge Ratios

The mean particle size was plotted as a function of the charge ratio. Error bars represent standard deviations.
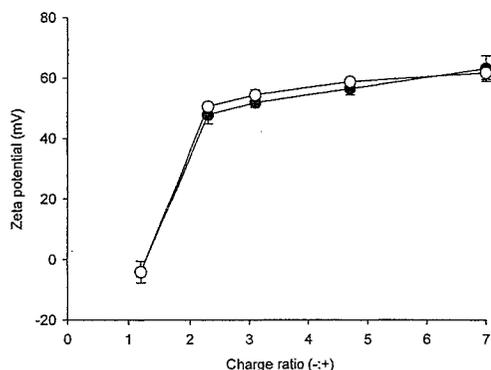

Fig. 2. The Zeta Potential of the Lipoplex (Open Circle) and Galactosylated Lipoplex (Closed Circle) at Different Charge Ratios

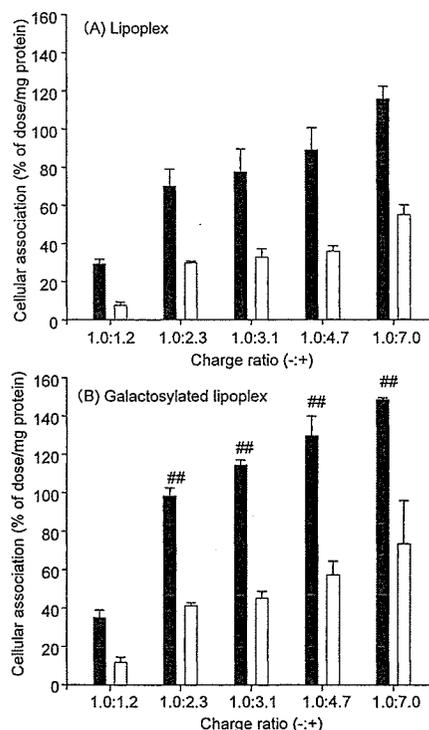The zeta potential was plotted as a function of the charge ratio. Error bars represent standard deviations.

Fig. 3. Cellular Association at 37 °C (Filled Bar) and 4 °C (Open Bar) of [32P]-Labeled-Plasmid DNA Lipoplex and Galactosylated Lipoplex at Different Charge Ratios after 3 h incubation in HepG2 cells

Error bars represent standard deviations. Statistically significant differences from lipoplex at 37 °C (##$p < 0.01$).
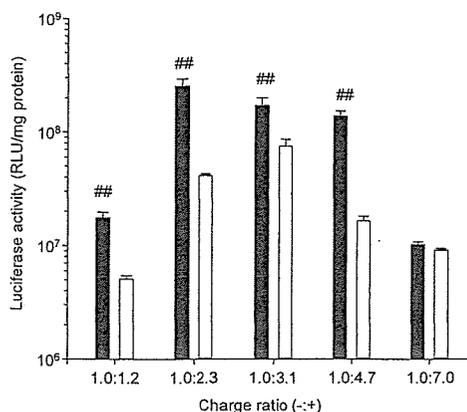
Fig. 4. Transfection Activity after Transfection by Lipoplex (Open Bar) and Galactosylated Lipoplex (Closed Bar) at Different Charge Ratio in HepG2 Cells

Error bars represent standard deviations. Statistically significant differences from lipoplex (## $p<0.01$).

Fig. 6. Cytotoxic Effect after Transfection by Lipoplex (Open Bar) and Galactosylated Lipoplex (Closed Bar) at Different Charge Ratio in HepG2 Cells

Cell growth was measured by MTT assay. Data represent the % of cell growth compared with untreated cells. Error bars represent standard deviations.
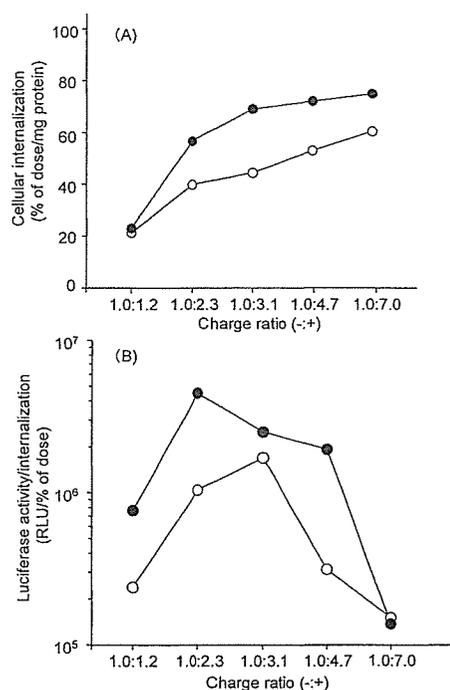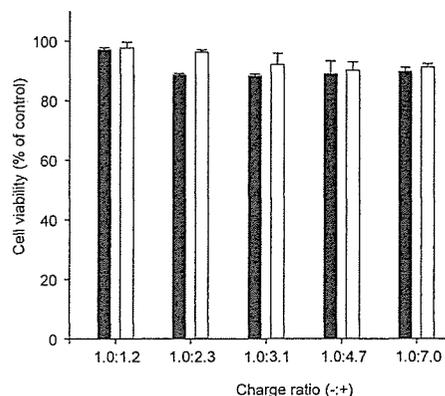

Fig. 5. Cellular Internalization (A) and Luciferase Activity/Cellular Internalization (B) after Transfection by Lipoplex (Open Bar) and Galactosylated Lipoplex (Closed Bar) at Different Charge Ratio in HepG2 Cells

Cellular internalization was calculated by the difference in the amount of $[^{32}P]$-labeled-plasmid DNA cellular association between 37 °C and 4 °C.

Cytotoxicity of Galactosylated Lipoplex To assess the relationship between cytotoxicity and gene expression efficiency, the cytotoxic effects of both lipoplexes were examined by MTT assay. Although there was a slight reduction in the amounts of formazan crystals in the cells, both lipoplexes exhibited no significant toxicity at any charge ratio (Fig. 6). There were no significant differences in the protein level and cell viability between these charge ratios after a 48 h incubation (data not shown).

DISCUSSION

The purpose of the present study was to investigate the major factors affecting transfection efficiency with galactosylated lipoplex in HepG2 cells. The particle size and zeta potential of both lipoplexes depended on the charge ratio (Figs. 1, 2). Since the particle size and zeta potential of both lipoplexes were almost identical at the same charge ratio, the effect of galactosylation of the lipoplex on cellular uptake, gene expression, and cytotoxicity could also be compared.

The uptake of galactosylated lipoplex was significantly higher than that of lipoplex, suggesting that the asialoglycoprotein receptor-mediated uptake was efficient by HepG2 cells. To investigate the gene expression characteristics of galactosylated lipoplex in HepG2 cells, the effect of the charge ratio (− : +) on gene expression was measured. Gene expression by galactosylated lipoplex was significantly higher than that by lipoplex at a charge ratio (− : +) of 1.0 : 1.2 to 1.0 : 4.7. These observations supported partially our previous report describing that galactosylated lipoplex was more efficiently taken up by HepG2 cells and/or hepatocytes via asialoglycoprotein receptors at a charge ratio (− : +) of 1.0 : 2.3.[8,15] In both lipoplexes, the highest gene expression was observed at a charge ratio (− : +) of 1.0 : 2.3 and transfection efficacy was reduced at higher charge ratios. This observation agrees with the previous reports about conventional lipoplex in various types of cells,[16,17] sterylglucoside-containing lipoplex in HepG2 cells,[18] and mannosylated lipoplex in macrophages by the uptake of mannose receptor.[19]

As shown in Fig. 4, the optimal charge ratio for gene ex-

estimated the amount of internalized plasmid DNA by subtracting the amount of adsorbed plasmid DNA on the cell surface at 4 °C from the amount of cell-associated plasmid DNA at 37 °C, assuming that the amounts adsorbed at both temperatures were the same. The calculated amount of plasmid DNA taken up by the cells also increased as the charge ratio (− : +) of both lipoplexes increased (Fig. 5A). Then, luciferase activity was dividing by internalization amount. The transfection efficacy per internalization amount of galactosylated lipoplex and lipoplex was the highest at the charge ratio (− : +) of 1.0 : 2.3 and 1.0 : 3.1, respectively (Fig. 5B).

pression was 1.0 : 2.3. However, the cellular association of plasmid DNA at 4 and 37 °C increased in parallel with the charge ratio of both lipoplexes (Fig. 3). Both lipoplexes bind to the cell surface due to an electrostatic interaction between the positive charges of the cationic liposomes and the negative charges on the cell surface.[11] Therefore, it is likely that the increased zeta potential of the complex at higher charge ratios will result in enhanced DNA cellular association. Taking these factors into consideration, the intracellular trafficking, rather than the degree of uptake of galactosylated lipoplex, is the key process for gene expression.

The cellular association and gene expression of galactosylated lipoplex at a charge ratio of 1.0 : 1.2 were relatively lower than those of other charge ratios and of the lipoplex (Figs. 3, 4). We previously reported that the galactose density of galactosylated liposomes is important for both effective recognition by asialoglycoprotein receptors and cell internalization in vivo.[20] Therefore, more galactose might be required on the surface of the lipoplex for efficient recognition by asialoglycoprotein receptors on HepG2 cells. At a charge ratio of 1.0 : 1.2, the transfection activity of galactosylated lipoplex was significantly higher than that of lipoplex although the cellular association was similar. Mammalian cells express several types of lectins involved in intracellular trafficking, including endocytosis, interorganelle routing and putative nuclear transport.[21] Recently, Klink et al. reported that lactosylated poly-L-lysine/plasmid DNA complex could localized in the nucleus by targeting a potential lectin-like protein with galactose/lactose specificity.[22] More recently, Wada et al. suggested a similar mechanism to explain the high transfection obtained using a galactosylated dendrimer/α-cyclodextrin conjugate.[23] These observations suggest that the transfection activity of galactosylated lipoplex is efficiently transported to the nucleus for efficient gene expression. Further studies are needed to clarify the mechanism governing the efficient nuclear localization by galactosylated lipoplex.

It has been suggested that the inhibition of transfection efficiency at higher charge ratios is most likely due to cytotoxicity in a series of in vitro transfection experiments.[1,24] Although there was a slight reduction in the amounts of formazan crystals in the other cells, the lipoplex exhibited no significant toxicity at any charge ratio (Fig. 6). Therefore, cytotoxicity does not play a major role in determining the optimal charge ratio in both forms of lipoplex-mediated transfection performed under our experimental conditions in HepG2 cells.

In conclusion, it is suggested that intracellular trafficking, rather than the degree of uptake and cytotoxicity, is the important process that determines the optimal charge ratio of galactosylated lipoplex in HepG2 cells. The information in this study will be valuable for the future use, design, and development of more efficient galactosylated lipoplexes for hepatocyte-selective gene transfer via asialoglycoprotein receptor-mediated endocytosis.

REFERENCES

1) Felgner P. L., Gadek T. R., Holm M., Roman R., Chan H. W., Wenz M., Northrop J. P., Ringold G. M., Danielsen M., *Proc. Natl. Acad. Sci. U.S.A.*, **84**, 7413—7417 (1987).
2) Liu Y., Liggitt D., Zhong W., Tu G., Gaensler K., Debs R., *J. Biol. Chem.*, **270**, 24864—24870 (1995).
3) Kawakami S., Ito Y., Fumoto S., Yamashita F., Hashida M., *J. Gene Med.*, **7**, 1526—1533 (2005).
4) Li W., Ishida T., Okada Y., Oku N., Kiwada H., *Biol. Pharm. Bull.*, **28**, 701—706 (2005).
5) Wu G. Y., Wu C. H., *J. Biol. Chem.*, **263**, 14621—14624 (1988).
6) Sun X., Hai L., Hu H. Y., Zhang Z. R., *J. Drug Target.*, **13**, 121—128 (2005).
7) Kim T. H., Kim S. I., Akaike T., Cho C. S., *J. Control. Release*, **105**, 354—366 (2005).
8) Kawakami S., Fumoto S., Nishikawa M., Yamashita F., Hashida M., *Pharm. Res.*, **17**, 306—313 (2000).
9) Fumoto S., Kawakami S., Ito Y., Shigeta K., Yamashita F., Hashida M., *Mol. Ther.*, **10**, 719—729 (2004).
10) Fumoto S., Kawakami S., Shigeta K., Higuchi Y., Yamashita F., Hashida M., *J. Pharmacol. Exp. Ther.*, **315**, 484—493 (2005).
11) Sakurai F., Inoue R., Nishino Y., Okuda A., Matsumoto O., Taga T., Yamashita F., Takakura Y., Hashida M., *J. Control. Release*, **66**, 255—269 (2000).
12) Farhood H., Serbina N., Huang L., *Biochim. Biophys. Acta*, **1235**, 289—295 (1995).
13) Kawakami S., Yamashita F., Nishikawa M., Takakura Y., Hashida M., *Biochem. Biophys. Res. Commun.*, **252**, 78—83 (1998).
14) Yang J. P., Huang L., *Gene Ther.*, **5**, 380—387 (1997).
15) Fumoto S., Nakadori F., Kawakami S., Nishikawa M., Yamashita F., Hashida M., *Pharm. Res.*, **20**, 1452—1459 (2003).
16) Felgner J. H., Kumar R., Sridhar C. N., Wheeler C. J., Tsai Y. J., Border R., Ramsey P., Martin M., Felgner P. L., *J. Biol. Chem.*, **269**, 2550—2561 (1994).
17) Yang J. P., Huang L., *Gene Ther.*, **4**, 950—960 (1997).
18) Hwang S. H., Hayashi K., Takayama K., Maitani Y., *Gene Ther.*, **8**, 1276—1280 (2001).
19) Kawakami S., Sato A., Nishikawa M., Yamashita F., Hashida M., *Gene Ther.*, **7**, 292—299 (2000).
20) Managit C., Kawakami S., Yamashita F., Hashida M., *J. Pharm. Sci.*, **94**, 2266—2275 (2005).
21) Monsigny M., Rondanino C., Duverger E., Fajac I., Roche A. C., *Biochim. Biophys. Acta*, **1673**, 94—103 (2004).
22) Klink D. T., Chao S., Glick M. C., Scanlin T. F., *Mol. Ther.*, **3**, 831—841 (2001).
23) Wada K., Arima H., Tsutsumi T., Hirayama F., Uekama K., *Biol. Pharm. Bull.*, **28**, 500—505 (2005).
24) Gao X., Huang L., *Biochem. Biophys. Res. Commun.*, **179**, 280—285 (1991).

informa
healthcare

Basic fibroblast growth factor-binding peptide as a novel targeting ligand of drug carrier to tumor cells

TAKESHI TERADA, MIKI MIZOBATA, SHIGERU KAWAKAMI, YOSHIYUKI YABE, FUMIYOSHI YAMASHITA, & MITSURU HASHIDA

Department of Drug Delivery Research, Graduate School of Pharmaceutical Sciences, Kyoto University, Kyoto 606-8501, Japan

Abstract

Drug systems targeting tumor cells using basic fibroblast growth factor (bFGF) have been widely reported. In this study, the peptide KRTGQYKLC (bFGFp), containing cysteine at the carboxyl termination of the bFGF-derived peptide, was applied as a novel ligand targeting tumor cells. bFGFp was conjugated with bovine serum albumin (BSA) and liposomes. The peptide was shown to inhibit the binding of bFGF to FGF receptor-1 (FGFR1). Interestingly, the binding study using surface plasmon resonance (SPR) assay revealed that the bFGFp–BSA was not bound to FGFR1, but was selectively bound to bFGF. Furthermore, the SPR assay showed that bFGFp–BSA is capable of binding to FGFR1 following the pretreatment with bFGF. The confocal microscopy study indicated that the uptake of bFGFp–BSA by NIH3T3 cells, which highly express FGFRs, was significantly enhanced by pretreatment with bFGF. Then, PEGylated liposomes containing bFGFp (bFGFp–liposome) were prepared by conjugating maleimide-PEG-PE with bFGFp. Following the pretreatment of bFGF, the uptake of bFGFp–liposomes by NIH3T3 cells was significantly enhanced. These results suggest that bFGFp–BSA and bFGFp–liposomes are taken by NIH3T3 cells via binding with bFGF. In addition, both bFGFp–BSA and bFGFp–liposomes had no effect on the proliferation of NIH3T3 cells. This strategy can be used as a novel system for targeting tumors highly expressing FGFRs without a proliferation effect.

Keywords: *Basic fibroblast growth factor, targeting, liposome, surface plasmon resonance assay*

Introduction

Basic fibroblast growth factor (bFGF) is a multi-functional protein which has mitogenic, chemotactic and angiogenic activities (Lappi 1995; Compagni et al. 2000). Several recent reports have demonstrated an autocrine role for bFGF in tumor cells (Halaban et al. 1987; Halaban et al. 1988; Dow and deVerre White 2000). Therefore, bFGF and their receptors (FGFRs) are especially produced by a variety of tumor cells and lead to tumor angiogenesis and progression (Klagsbrun et al. 1986; Takanami et al. 1996; Volm et al. 1997). It has recently been reported that the overexpression of FGFRs in tumor cells can be used to achieve successful drug targeting. Targeting of FGFRs by toxin-conjugated or fused bFGF–saporin (a ribosome-inactivating protein) could control the proliferation of tumor cells that highly express FGFRs

(Beitz et al. 1992; Ying et al. 1994; Davol and Frackelton 1999). In addition, bFGF retargeted adenovirus (Hoganson et al. 2001; Kleeff et al. 2002; Qin et al. 2005) and the conjugated polylysine with bFGF (Sosnowski et al. 1996; Hoganson et al. 1998) have exhibited high expression in tumor cells with up-regulated FGFRs.

However, bFGF itself is potent inducer of angiogenesis. Although the cell-surface receptors on tumor cells possess intrinsic tyrosine kinase activity and are phosphorylated upon binding of bFGF (Burgess and Maciag 1989; Klagsbrun 1989), bFGF is able to stimulate tumor proliferation, migration and differentiation and/or to induce angiogenesis. Recently, it was reported that bFGF infusion resulted in significant increases in tumor vascularity, blood flow and growth (Gross et al. 1993; Davies et al. 2002). Therefore, since a drug delivery system using

Correspondence: M. Hashida, Department of Drug Delivery Research, Graduate School of Pharmaceutical Sciences, Kyoto University, Kyoto 606-8501, Japan. Tel: 81 75 753 4525. Fax: 81 75 753 4575. E-mail: hashidam@pharm.kyoto-u.ac.jp

bFGF as the targeting ligand can induce proliferation of tumor cells that up-regulate FGFR, a targeting ligand without any proliferation effect is needed.

Recently, Yayon et al. (1993) identified bFGF-derived peptide KRTGQYKL (residues 119–126 of bFGF) as inhibitor of the binding between bFGF and its receptor following examination of a random phage-epitope library. Furthermore, this peptide itself had no tumor proliferation effects and inhibited the proliferation of bovine aortic endothelial cells in complete growth medium.

In this study, bFGF-derived peptide KRTGQYKL was conjugated with bovine serum albumin (BSA) and its cellular binding characteristics were investigated. Sulfo-succinimidyl-4-(N-maleidomethyl) cyclohexane-1-carboxylate (sulfo-SMCC), which is a general reagent for connection via surface amino residues to the other molecules with thiolated moieties, was used as a linker between the peptide and BSA. To obtain the conjugate with BSA, we prepared KRTGQYKLC (bFGFp) containing cysteine at the carboxyl terminal and conjugated bFGFp with BSA via the surface amino residues. Surface plasmon resonance (SPR) spectroscopy, which allows real-time detection of macromolecular interactions without using radioactive or fluorescent labeled ligands, was used for this study to confirm the binding of bFGFp–BSA. In addition, we prepared bFGFp–liposomes containing conjugated maleimide-PEG-PE with the peptide and evaluated this strategy, since liposomes have been widely investigated as drug delivery systems (Hashida et al. 2005).

Here, we demonstrate the characteristics of bFGFp–BSA and bFGFp–liposomes as a drug delivery system by an *in vitro* study using NIH3T3 and FGFRs-deficient Chinese hamster ovary (CHO-K1) cells (Rusnati et al. 2002). Interestingly, bFGFp–BSA exhibited high binding to bFGF, but not FGFR1. As far as the uptake characteristics are concerned, bFGFp–BSA exhibited a higher uptake via bFGF in NIH3T3 cells, which express a considerable amount of FGFRs. Based on these findings, we developed novel bFGFp-modified liposomes for tumor-selective drug delivery. In the presence of bFGF, bFGFp-modified liposomes exhibit a higher uptake via bFGF in NIH3T3 cells. Since bFGFp itself has no tumor proliferation effects, bFGFp is an effective potential targeting ligand for targeted delivery to tumor cells.

Materials and methods

Materials

Sulfo-SMCC was purchased from Pierce Biotechnology Inc. (Rockford, IL, USA). Recombinant human bFGF was obtained from PeproTech EC. (London, UK). Recombinant human FGFR1α(IIIc)/Fc chimera was purchased from Techne Co. (Minneapolis, MN, USA). Distearoyl phosphatidylcholine (DSPC), cholesteryl chloroformate and 3-(4,5-dimethylthiazol-2-yl)-2,5-diphenyltetrazolium bromide (MTT) were purchased from Sigma-Aldrich Co. (St Louis, MO, USA). Cholesterol (Chol) and Clear-Sol I were obtained from Nacalai Tesque Inc. (Kyoto, Japan) and Soluene 350 was purchased from Packard Bioscience Co. (Groningen, Netherlands). $[^3H]$ CHE was purchased from NEN Life Science Products Inc. (Boston, MA, USA). The peptide KRTGQYKLC (bFGFp) was custom-made by Toray Research Center Inc. (Tokyo, Japan). mPEG$_{3000}$-DSPE was purchased from Avanti Polar Lipids Inc. (Alabama, AL, USA) and Maleimide-PEG$_{2000}$-DSPE was purchased from NOF Co. Inc. (Tokyo, Japan). Dulbecco's-modified Eagle's minimum essential medium (DMEM) and Hank's buffered salt solution (HBSS) were obtained from Nissui Pharmaceutical Co. Ltd. (Tokyo, Japan). Fetal bovine serum (FBS) was obtained from Biowhittaker Co. (Walkersville, MD). All other chemicals were reagent grade products obtained commercially.

Synthesis of bFGFp–BSA

bFGFp–BSA was synthesized according to the method reported previously (Backstrom and Sander-Bush 1997). bFGFp containing cysteine at the carboxyl terminal of bFGF-derived peptide KRTGQYKL was prepared for this synthesis. The SMCC derivatives of BSA were obtained by simultaneous addition of 20 mg BSA and 2.5 mg sulfo-SMCC to 2.0 ml 0.05 M carbonate buffer at pH 8.5 while stirring. After 1 h at room temperature, the mixture was centrifuged by VIVA SPIN 10 kDa cut-off (VIVASCIENCE, Hannover, Germany) to remove any unreacted sulfo-SMCC and then the buffer was changed to distilled water and the solution was lyophilized. Subsequently, 10 mg of the synthetic SMCC–BSA was incubated with 2.0 mg bFGFp in PBS (1.0 ml). After 3 h at 4°C, the mixture was centrifuged by VIVA SPIN to remove unreacted peptide, followed by dialysis and lyophilization. The number of conjugated SMCC and peptide groups was calculated from the number of free amino acid groups determined by trinitrobenzene sulfonic acid using BSA as a standard (Habeeb 1966). Furthermore, the 10 mM L-cysteine solution and the product were mixed at room temperature for 1 h to remove the free maleimide, followed by dialysis and lyophilization.

Synthesis of bFGFp–PEG-DSPE

bFGFp (28 mg, 26 μmol) was dissolved in 0.1 M HEPES buffer (pH 7.0, 2 ml). Maleimide-PEG$_{2000}$-DSPE (50 mg, 17 μmol) and methanol (0.2 ml) were added to the bFGFp solution at 4°C while stirring.

The reaction was continued at 4°C for 2 days. The mixed solution was dialyzed against distilled water and lyophilized. TLC analysis and ninhydrin assay showed the disappearance of free maleimide-PEG_{2000}-DSPE and the appearance of bFGFp–PEG-DSPE, which indicates that the reaction had gone to completion. The purity of the synthetic bFGFp–PEG-DSPE was determined by fluorescamine assay (Bohlen et al. 1973) and found to be over 90% on the basis of the amino acid content of bFGFp. Furthermore, 10 mM L-cysteine solution and the product were mixed at room temperature for 1 h to remove the free maleimide-PEG_{2000}-DSPE, followed by dialysis and lyophilization.

Preparation of liposomes

Liposomes were prepared by our previously reported method (Kawakami et al. 2000; Kawakami et al. 2001; Managit et al. 2005a). Each lipid mixture (DSPC, Chol, and $mPEG_{3000}$-DSPE) and [^{3}H] CHE were dissolved in chloroform and evaporated to dryness. bFGFp–PEG-DSPE was solved in mixed organic solvent (chloroform: methanol = 1:1) beforehand. The dried lipid films were hydrated in HBSS, sonicated at 65°C for 3 min and then extruded through polycarbonate filters with a pore size of 0.2 μm. Mean particle diameters were determined by laser light scattering using a Zetasizer Nano ZS (Malvern Instruments, Malvern, UK). All liposomes were similar in size (an average diameter of approximately 100 nm) as shown in Table I.

SPR spectroscopy assay

SPR measurements were performed using a BIAcore X (BIAcore, Uppsala, Sweden). bFGFp–BSA or FGFR1 was immobilized on the surface of a CM5 sensor chip using the standard amine coupling procedure of the manufacturer. Briefly, the surface of the chip consisting of flow cells 1 and 2 was activated by exposing them to a mixture of 0.05 M N-hydroxysuccinimide (NHS) and 0.2 M N-ethyl-

N'-dimethyl aminopropyl carbodiimide (EDC) for 7 min. Flow cell 1 was immobilized with bFGFp–BSA or FGFR1 in acetate buffer (pH 4.0). The immobilized amount of bFGFp–BSA and FGFR1 were approximately 8000 and 5000 resonance units (RU), respectively. Flow cell 2 was immobilized using the same amount as for flow cell 1 by BSA to be used as a blank sensorgram for subtraction of the bulk refractive index background. Finally, the unreacted sites of both immobilized flow cell were blocked with 0.1 M ethanolamine (pH 8.5). All reagents were injected at a flow rate of 5.0 μl/min.

Each sample was adjusted to an appropriate concentration using a running buffer (150 mM NaCl, 10 mM HEPES, pH 7.4). The mixed solution of bFGF and bFGFp or bFGF and bFGFp–BSA was prepared 30 min before the SPR study. In all studies, each sample was allowed to flow at a rate of 10 μl/min at 25°C for 2 min and dissociated for 2 min. The regeneration of the sensor chip was carried out by injection of 10 μl 50 mM HCl.

The sensorgram was analyzed by a global fitting procedure using a 1:1 (Langmuir-type) binding model-derived equation that is available in the BIAevaluation 3.0 software. The dissociation constant (K_d) was determined from k_d/k_a.

Cellular association and visualization of FITC labeled bFGFp–BSA and BSA

SMCC–BSA and bFGFp–Cys–SMCC–BSA were labeled with FITC as previously described (Monsigny et al. 1984). Briefly, BSA before the modification of SMCC was incubated with three equivalents of FITC in 0.1 M sodium carbonate buffer, pH 9.5 solution by stirring for 5 h at room temperature. The mixture was centrifuged by VIVA SPIN to remove the unreacted FITC and then purified by dialysis with distilled water and lyophilized. The FITC–BSA was used for the modification of bFGFp as described above.

NIH3T3 cells were seeded on glass coverslips in 12-well plates at a density of 1 × 10^5 cells/well. After complete adhesion, the cells were washed 3-times with HBSS and incubated at 37°C for 2 h with each FITC-labeled protein (50 μg/ml) dissolved in HBSS. After incubation, the protein solution was removed and the cells were washed 3-times with HBSS, then fixed with 4% paraformaldehyde in PBS and incubated at room temperature for over 20 min. After washing twice with PBS, they were treated with 0.2% Triton X-100–PBS, 5 μg/ml RNase A and 0.5 μg/ml propidium iodide in 0.1 M Tris–HCl (pH 7.4) containing 0.1 M NaCl for nuclei staining. Then, they were mounted in glycerol:PBS (1:1) containing 2.5% 1,4-diazobicyclo (2,2,2) octane. Images were then obtained by confocal laser scanning microscopy (MRC-1024, Bio-Rad, Hercules, CA, USA).

Table I.   Lipid composition and mean particle size of liposomes investigated.

Lipid composition (molar ratio)	Particle size (nm)
DSPE/Chol/bFGFp–PEG-DSPE (60:30:10)	93 ± 2.21
DSPE/Chol/bFGFp–PEG-DSPE (60:35:5)	115 ± 7.61
DSPE/Chol/bFGFp–PEG-DSPE (60:37.5:2.5)	100 ± 1.76
DSPE/Chol/bFGFp–PEG-DSPE (60:39:1)	114 ± 1.99
DSPE/Chol/mPEG-DSPE (60:39:1)	101 ± 1.71

Results are expressed as the means ± SD of three experiments.

Cellular association experiments with [³H] CHE labeled bFGFp–liposomes

A cellular association study was performed using our previously reported method (Opanasopit et al. 2001; Managit et al. 2005b). Briefly, NIH3T3 and CHO-K1 cells were plated on 12-well culture plates at a density of 1×10^5 cells/well. After 24 h cultivation, the cells were washed 3-times with HBSS and incubated with each lot of treated [³H] CHE labeled liposomes (100 μM) in HBSS at 37°C. The pretreatment of each lot of liposomes by bFGF was carried out 30 min before the uptake study. After 2 h of incubation, the medium was removed and the cells were washed 5-times with HBSS. The cells were then solubilized with 0.5 ml 1.0 N NaOH solution overnight and then neutralized with 0.1 ml 5.0 N HCl solution. The radioactivity was measured in a scintillation counter (LSA-500, Beckman, Tokyo, Japan). The amount of cellular protein in each cell lysate was estimated using a protein quantification kit (Dojindo Molecular Technologies, Inc. Gaithersburg, MD, USA).

Cell proliferation assay

The effect on cell proliferation produced by bFGFp–BSA and –liposomes in presence or absence of bFGF was assessed by MTT assay (Mosmann 1983). Briefly, NIH3T3 cells were counted and seeded in 96-well plates at a density of 4×10^3 cells/well. After 24 h of incubation, the cells were exposed to samples diluted in DMEM without FBS. After 72 h of incubation, MTT assay was performed in triplicate.

Statistical analysis

Statistical comparisons were performed by Student's *t*-test for two groups. $P < 0.05$ was considered to be indicative of statistical significance.

Results

The interaction analysis of bFGFp–BSA with FGFR1 and bFGF

To clarify the characterization of the binding of bFGF-derived peptide KRTGQYKL with FGFR1 and bFGF, bFGFp containing cysteine at the carboxyl terminal of the peptide sequence was conjugated with BSA using sulfo-SMCC and the interaction was evaluated by SPR spectroscopy. The amount of incorporated bFGFp calculated from the amino acid groups was about 12 peptides per molecule of BSA.

The conjugated bFGFp–BSA was immobilized on the surface of a sensor chip CM5 by amine coupling. Non-specific binding of an analyte and any change in bulk refractive index were ruled out by immobilizing BSA as a control. Although the bFGFp-containing peptide sequence was reported to inhibit the

interaction between bFGF and FGFR1 (Yayon et al. 1993), no response signal was observed in FGFR1 (Figure 1(A)). However, bFGF exhibited a significantly high response signal and this response of bFGF was reduced in the presence of bFGFp. The binding of bFGF to bFGFp–BSA was completely regenerated by the injection of 50 mM HCl (Figure 1(B)), suggesting that the interaction does not involve chemical binding via any active groups. These results suggest that bFGFp–BSA does not bind to FGFR1, but binds to bFGF. The injected bFGF bound to bFGFp–BSA in a concentration-dependent manner and the dissociation was very slow, indicating that the binding affinity was high (Figure 1(C)). The association and
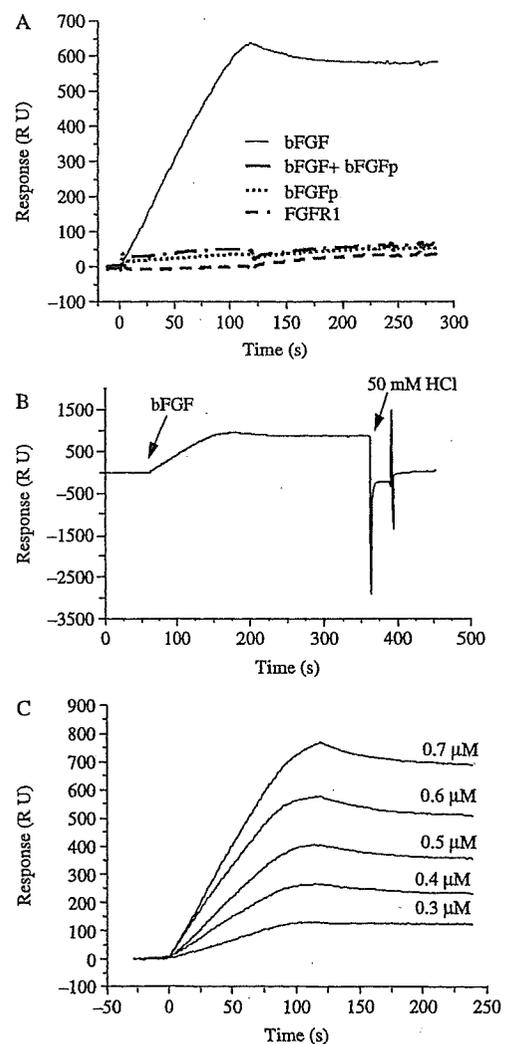

Figure 1. SPR sensorgrams of bFGF binding to bFGFp–BSA. (A) 10 μg/ml bFGF, the mixture of 10 μg/ml bFGF and 100 μg/ml bFGFp, 100 μg/ml bFGFp and 10 μg/ml FGFR1 were injected over immobilized bFGFp–BSA. (B) 10 μg/ml bFGF was injected onto the sensor chip. Subsequently, the sensor chip was completely regenerated by the injection 50 mM HCl. (C) Different concentrations of bFGF were injected over immobilized bFGFp–BSA. Each sensorgram was overlaid and zeroed on the *y*-axis to the average baseline. The start injection time for each sample was set to zero on the *x*-axis.

Table II. Rate constants and dissociation constants for the interaction between immobilized bFGFp–BSA and bFGF.

	Rate constants		Dissociation constant
	$k_a \times 10^{-3}$ $(M^{-1}s^{-1})$	$k_d \times 10^4$ (s^{-1})	$K_d \times 10^8$ (M)
bFGF	4.09 ± 0.727	4.83 ± 0.857	12.2 ± 3.52

Results are expressed as the means ± SD of three replicates.

dissociation rate constants were estimated by global fitting to sensorgrams using a 1:1 (Langmuir-type) binding model-derived equation. The calculated dissociation constant was $12.2 \pm 3.52 \times 10^{-8}$ M (Table II).

The binding of bFGFp–BSA to FGFR1 via bFGF

FGFR1 and BSA as a control were immobilized on the surface of a sensor chip CM5 by amine coupling as described above. Although bFGF showed a significantly high response signal (Figure 2), no response signal was observed with bFGFp–BSA, suggesting that bFGFp–BSA does not bind to FGFR1. In addition, the response signal of bFGFp–BSA pre-incubated with bFGF was much higher than that of bFGF itself, suggesting that bFGFp–BSA pre-incubated with bFGF is capable of binding to FGFR1 via bFGF.

The effect of bFGF on the uptake of bFGFp –BSA by NIH3T3 cells

The uptake of bFGFp–BSA by NIH3T3 cells, overexpressing FGFRs, was evaluated by confocal microscopy. FITC-labeled BSA or bFGFp–BSA was incubated with the cells in presence of bFGF or the mixture of bFGF with an excess of bFGFp. The uptake of bFGFp–BSA pre-incubated with bFGF was significantly higher than that of bFGF–BSA alone (Figure 3). However, in the case of BSA, there was no
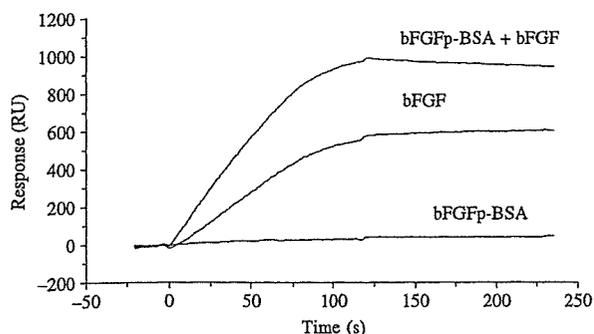

Figure 2. SPR sensorgram of binding of bFGFp–BSA to FGFR1 via bFGF. About 100 μg/ml bFGFp–BSA, 5 μg/ml bFGF and the mixture of 100 μg/ml bFGFp–BSA and 5 μg/ml bFGF were injected over the immobilized FGFR1.

difference when bFGF was present or not. The higher uptake was significantly reduced by the mixture of bFGF with an excess of bFGFp, suggesting that the increase in fluorescence in the cells of bFGFp–BSA pre-incubated with bFGF was due to the FGFR-mediated endocytosis.

The effect of bFGF on the uptake of bFGFp–liposomes by NIH3T3 cells

To further evaluate this strategy using bFGFp-conjugated delivery systems, we prepared liposomes containing different amounts of bFGFp–PEG$_{2000}$-DSPE conjugated maleimide-PEG-DSPE with bFGFp as a novel tumor-selective liposome. Table I summarizes the lipid composition and particle size of the liposomes prepared. All filtered liposomes were similar in size (average diameter approximately 100 nm). All pretreated bFGFp–liposomes with bFGF exhibited a higher uptake than the untreated group (Figure 4). In particular, in the condition with 1 μg/ml bFGF, 2.5 and 5.0% bFGFp–liposomes exhibited a high effect of bFGF in comparison with 1.0 and 10%. Furthermore, similar to bFGFp–BSA, bFGFp–liposomes tended to exhibit a high uptake even without the addition of bFGF, though the uptake was less than that of bFGFp–liposome with bFGF, and this was dependent on the amount of bFGFp–PEG$_{2000}$-DSPE. It suggests that bFGFp–liposome might indicate the cellular uptake not only by the interaction with FGFRs via binding to bFGF but also by the other cause.

The effect of bFGF on the uptake of bFGFp–liposomes by CHO-K1 cells

To determine whether the high uptake in NIH3T3 cells by the addition of bFGF is via FGFRs, the uptake study was also conducted using FGFRs-deficient CHO-K1 cells. The addition of bFGF did not enhance the uptake of 5.0 and 10% bFGFp–liposomes, but inhibited it (Figure 5(A)). In addition, the inhibition was dependent on the concentration of the added bFGF (Figure 5(B)). These results support the hypothesis that bFGFp–liposomes are capable of binding to bFGF and the effect of bFGF in NIH3T3 cells may be due to the uptake via FGFRs.

The effect of bFGFp-conjugated delivery systems on the viability and proliferation of NIH3T3 cells

bFGF is known to exhibit a strong proliferative effect on most tumor cells. To determine the effect of bFGFp-conjugated delivery systems on the viability and proliferation of tumor cells, NIH3T3 cells were incubated with bFGFp, bFGFp–BSA, and bFGFp–liposomes in the absence or presence of 1 nM bFGF (Figure 6(A),(B)). In this study, 0.72 and
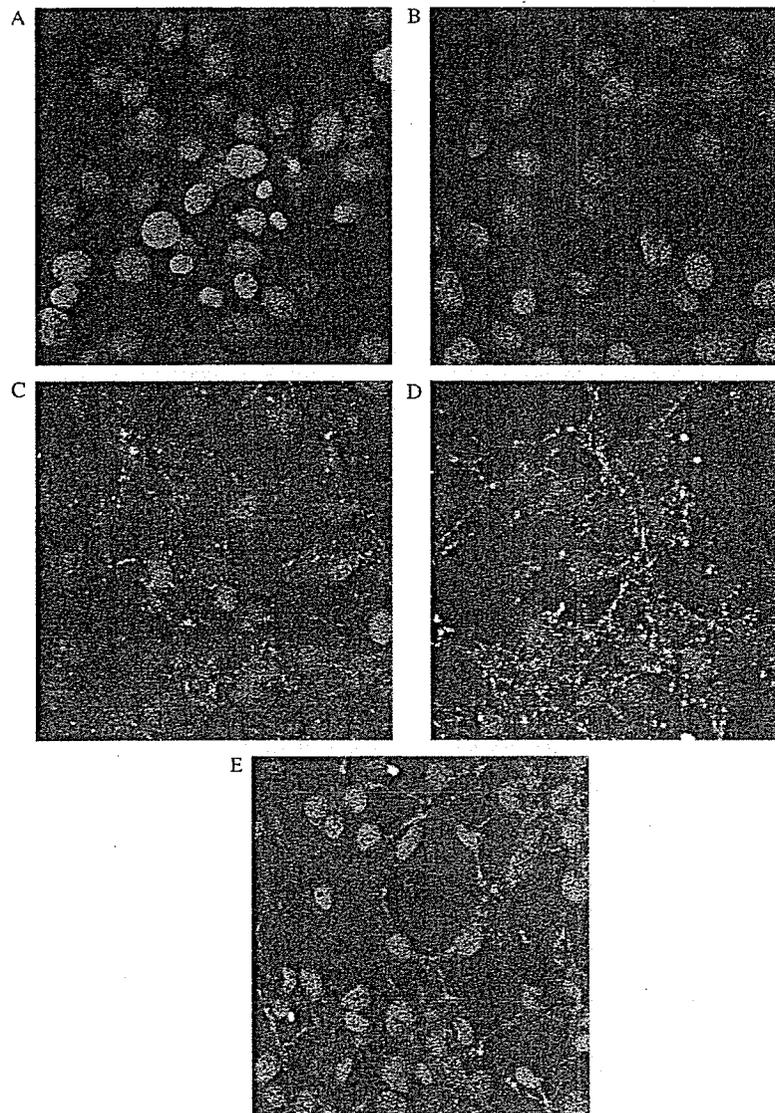
Figure 3. Confocal microscopy of FITC–BSA and FITC–bFGFp–BSA preincubated with bFGF in NIH3T3 cells. NIH3T3 cells were incubated with FITC–BSA (A), a mixture of FITC–BSA and bFGF (B), FITC–bFGFp–BSA (C), a mixture of FITC–bFGFp–BSA and bFGF (D), and a mixture of FITC–bFGFp–BSA, bFGF and bFGFp (E) at 37°C for 2 h. Red signals indicate the nuclei stained with propidium iodide.

7.2 μg/ml bFGFp–BSA and 4.0 and 40 μM bFGFp–liposomes contained 0.1 and 1.0 μM of conjugated bFGFp, respectively. The incubation with an excess of bFGFp, bFGFp–BSA and bFGFp–liposomes had no cell proliferation of cells in the absence of bFGF. Furthermore, in the presence of bFGF, the incubation had no influence on the proliferation by bFGF, although bFGFp is capable of binding to bFGF.

Discussion

The bFGF-derived peptide KRTGQYKL (residues 119–126 of bFGF) has been reported to inhibit the binding of bFGF to FGFR1 (Yayon et al. 1993) and to have no cell proliferation effect. Since FGFRs are overexpressed on the surface of many tumor cells, we

hypothesized that the conjugated peptide carrier would be capable of delivering antitumor drugs to tumor cells via direct binding to FGFRs, without inducing any tumor growth.

To examine the binding ability, we firstly prepared bFGFp–BSA-conjugated BSA to the peptide using sulfo-SMCC and evaluated this compound using SPR spectroscopy, which has been widely used as a tool to study biomolecular interactions including those between receptors and ligands (Wu and Chaiken 2004), DNA–protein (Wegner et al. 2003; Schubert et al. 2003) and protein–protein interactions (Stenlund et al. 2003). Although FGFR1 exhibited no binding to the immobilized bFGFp–BSA, bFGF showed a specific interaction via the presence of bFGFp on the surface of BSA (Figure 1). Although these results were different from our hypothesis, the
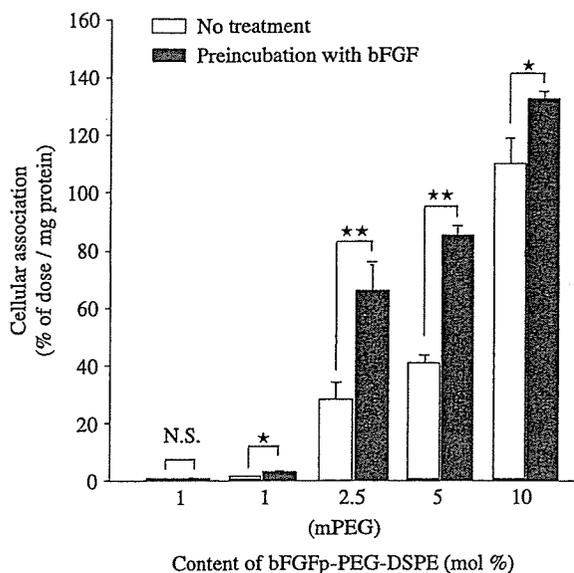
Figure 4.   The uptake of [³H]mPEG-liposomes and [³H]bFGFp–liposomes containing different amounts of bFGFp–PEG-DSPE (100 μM) with (■) and without 1 μg/ml bFGF (□) for 2 h by NIH3T3 cells. Results are expressed as the mean ± SD values (*n* = 3). Statistical analysis was performed by Student's *t*-test (**, *P* < 0.01; *, *P* < 0.05; NS, not significant).

interaction between bFGF-derived peptide and bFGF could be explained by the oligomeric self-association of bFGF (Venkataraman et al. 1996; Davis et al. 1999). Safran et al. (2000) showed that the essential residues of bFGF allow inter-monomer interactions that stabilize the bFGF dimer. The used peptide (KRTGQYKL) in this study is included in the sequence contributing to the construction of the bFGF dimer or oligomer. Taking these facts into consideration, the peptide may bind to bFGF via the sequence involved in bFGF self-association.

As shown in Figure 2, we found that bFGFp–BSA binds to FGFR1 via bFGF and this result suggests that the binding site of bFGF to bFGFp–BSA is different from that of FGFR1. This observation agrees with the report by Davis et al. (1999) who found that there are separate sites for bFGF self-association and receptor binding on the surface of bFGF. Therefore, it suggests that the binding bFGF to bFGFp–BSA would inhibit the intact interaction between the bFGF and FGFR1. Tumor cells, such as melanoma, breast cancer and prostate cancer, are reported to exhibit overexpression of bFGF and FGFRs (Penault-Llorca et al. 1995; Danielsen and Rofstad 1998; Kwabi-Addo et al. 2004). Furthermore, such tumor tissues possess high concentrations of bFGF (Giri et al 1999). Furthermore, the low dissociation constant of the interaction between bFGFp–BSA and bFGF suggests the possibility of a novel targeting strategy (Table II). Therefore, our observations suggest that the conjugated peptide carrier would be capable of delivering antitumor drugs to tumor cells with FGFRs via binding to bFGF.
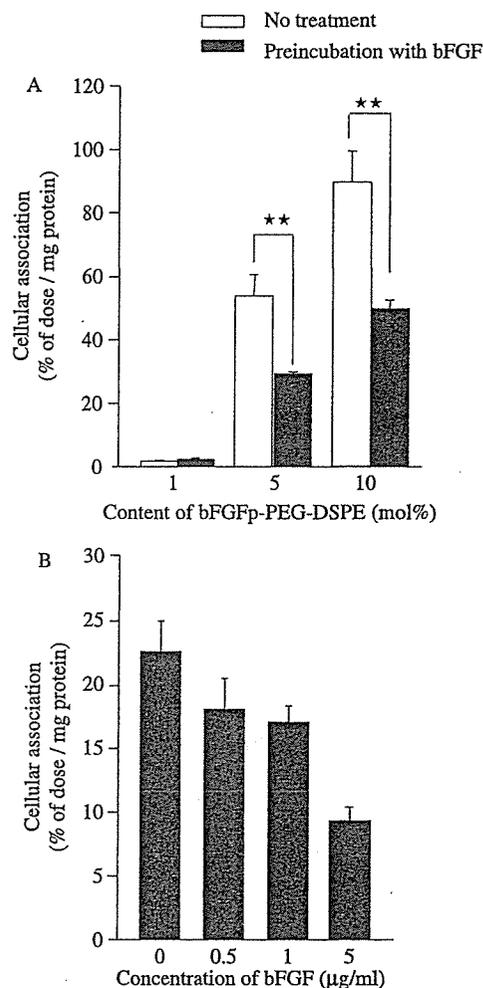
Figure 5.   The uptake of [³H]bFGFp–liposomes with (■) and without 1 μg/ml bFGF (□) for 2 h by CHO-K1 cells. (A) The effect of the amount of bFGFp–PEG-DSPE contained in bFGFp–liposomes was investigated. (B) The effect of the concentration of bFGF preincubated with 2.5% bFGFp–liposome was investigated. Results are expressed as the mean ± SD values (*n* = 3). Statistical analysis was performed by Student's *t*-test (**, *P* < 0.01).

The receptor-mediated internalization allows the liposomes to avoid the action of multi drug resistant (MDR) transporters like *P*-glycoprotein (Sapra and Allen 2003). Therefore, the internalization of drug carrier in the tumor cells allows an enhancement of the pharmacological effects of the antitumor drug. Some groups have reported that bFGF binding to FGFRs is internalized and translated to the nucleus, subsequently inducing cell proliferation (Baldin et al. 1990; Olsnes et al. 2003; Soulet et al. 2005). Our confocal microscopy study revealed that bFGF enhances the internalization of bFGFp–BSA (Figure 3). In contrast, this effect was not observed in the case of BSA. Furthermore, pretreatment by the mixture of bFGFp and bFGF did not enhance the internalization via exogenous bFGF. These results provide evidence that the increase in the internalization by bFGF is due to the binding of bFGFp–BSA
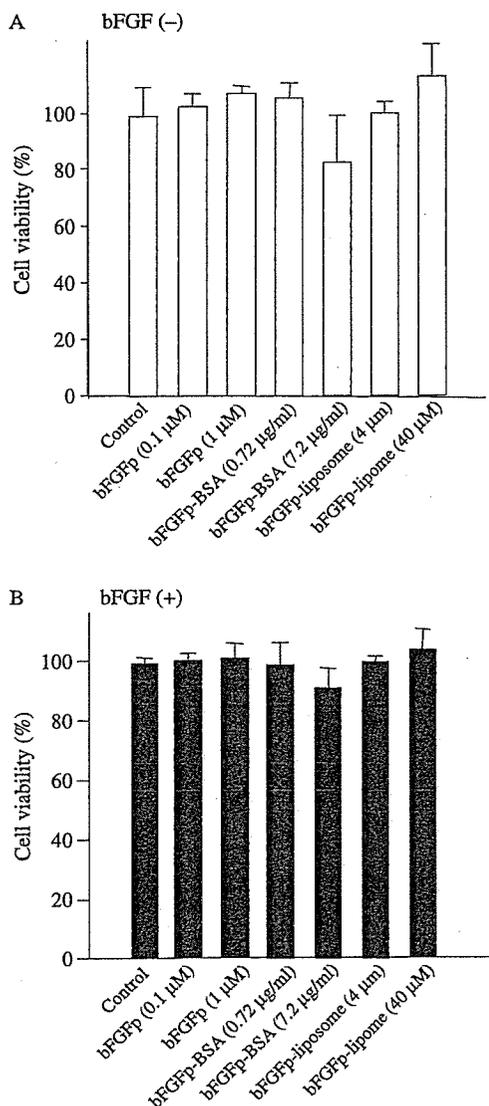
Figure 6. Effects of bFGFp and the drug delivery system using bFGFp on the cell viability of NIH3T3 cells without (A) and with (B) 1 nM bFGF. Each bFGFp and drug delivery system, following adjustment to the appropriate concentration, were added to NIH3T3 cells. After 72 h, the cell viability was investigated by MTT assay. Each value represents the mean ± SD values ($n = 3$).

to FGFRs expressed by NIH3T3 cells via bFGF and not due to the physiological effect of bFGF itself.

Liposomes have been widely investigated as drug delivery carriers. The modification by targeting ligand to the PEG terminal results in PEG-liposomes exhibiting both prolonged circulation and effective target binding. Therefore, bFGFp–liposomes with bFGFp on the PEG terminus were prepared and evaluated as a novel ligand to target tumor cells. Following the addition of bFGF, the uptake of liposomes containing different amounts of bFGFp–PEG-DSPE by NIH3T3 cells was enhanced similar to bFGFp–BSA (Figure 4). In particular, bFGFp–liposomes containing 2.5 and 5.0% bFGFp–PEG-DSPE exhibited and increased uptake following

the addition of bFGF. However, the increase in the uptake of PEG-liposomes following the addition of bFGF was barely detectable, indicating that the binding of the peptide in bFGFp–liposomes to bFGF is essential for enhanced uptake.

In order to investigate whether bFGFp–liposomes bound to bFGF are taken up via FGFRs in NIH3T3 cells, the uptake using CHO-K1 cells, deficient in FGFRs (Rusnati et al. 2002), was examined. Unlike the case of NIH3T3 cells, pretreatment by bFGF resulted in no increase in uptake, rather a reduction in CHO-K1 cells (Figure 5). Furthermore, the uptake decreased according to the concentration of bFGF used for pretreatment. These results suggest that the unexpected uptake of bFGFp–liposomes in CHO-K1 cells is inhibited by binding to bFGF. These observations suggest that the increased uptake by NIH3T3 cells is due to uptake via FGFRs.

Although bFGF enhanced the proliferation effect of NIH3T3 cells overexpressing FGFRs, incubation with an excess of bFGFp–BSA, bFGFp–liposome and bFGFp alone produced no proliferation effect (Figure 6(A)). Therefore, it is expected that bFGFp–liposomes do not induce tumor cell proliferation. In addition, regardless of the binding of bFGF to conjugated carriers by bFGFp, bFGF in the presence of an excess of conjugated carriers exhibits the same proliferation effect as bFGF alone (Figure 6(B)). The result shows that the binding to bFGFp–liposomes has no effect on the proliferation produced by bFGF and supports the view that bFGFp–liposome binding to bFGF might be recognized by FGFRs.

In all studies, an unexpected uptake without the addition of bFGF was observed. bFGFp–liposomes exhibited unexpected uptake in NIH3T3 and CHO-K1 cells and the effect increased according to the amount of bFGFp–PEG-DSPE. One possible explanation of this is that the cationic nature of bFGFp might induce unexpected binding to the cells. Another explanation is that bFGFp might bind to any receptor on the surface of the cells. The screening of functional peptides without unexpected binding may allow the successful application of this strategy. Alternatively, the incorporation into bFGFp–liposomes of PE-PEG with a short enough length to reduce the unexpected binding may enhance the targeting efficiency to FGFRs via bFGF. Immunoliposomes incorporating PE-PEG have been reported to prolong blood circulation in the body (Maruyama 2002).

In summary, the current studies demonstrated that bFGFp is capable of binding to bFGF and the bFGFp/bFGF is able to bind to FGFR. Furthermore, the drug delivery system using bFGFp was taken up in the cells overexpressing FGFRs via binding to bFGF. Although some problems still need to be overcome, this finding provides new information to help in the development of safe and effective drug delivery system targeting tumor cells.

References

Backstrom JR, Sanders-Bush E. 1997. Generation of anti-peptide antibodies against serotonin 5-HT2A and 5-HT2C receptors. J Neurosci Methods 77:109–117.

Baldin V, Roman AM, Bosc-Bierne I, Amalric F, Bouche G. 1990. Translocation of bFGF to the nucleus is G1 phase cell cycle specific in bovine aortic endothelial cells. EMBO J 9:1511–1517.

Beitz JG, Davol P, Clark JW, Kato J, Medina M, Frackelton AR, Jr, Lappi DA, Baird A, Calabresi P. 1992. Antitumor activity of basic fibroblast growth factor–saporin mitotoxin in vitro and in vivo. Cancer Res 52:227–230.

Bohlen P, Stein S, Dairman W, Udenfriend S. 1973. Fluorometric assay of proteins in the nanogram range. Arch Biochem Biophys 155:213–220.

Burgess WH, Maciag T. 1989. The heparin-binding (fibroblast) growth factor family of proteins. Annu Rev Biochem 58:575–606.

Compagni A, Wilgenbus P, Impagnatiello MA, Cotten M, Christofori G. 2000. Fibroblast growth factors are required for efficient tumor angiogenesis. Cancer Res 60:7163–7169.

Danielsen T, Rofstad EK. 1998. VEGF, bFGF and EGF in the angiogenesis of human melanoma xenografts. Int J Cancer 76:836–841.

Davies MM, Burke D, Carnochan P, Glover C, Kaur S, Allen-Mersh TG. 2002. Basic fibroblast growth factor infusion increases tumour vascularity, blood flow and chemotherapy uptake. Acta Oncol 41:84–90.

Davis JC, Venkataraman G, Shriver Z, Raj PA, Sasisekharan R. 1999. Oligomeric self-association of basic fibroblast growth factor in the absence of heparin-like glycosaminoglycans. Biochem J 341:613–620.

Davol PA, Frackelton AR, Jr. 1999. Targeting human prostatic carcinoma through basic fibroblast growth factor receptors in an animal model: Characterizing and circumventing mechanisms of tumor resistance. Prostate 40:178–191.

Dow JK, deVere White RW. 2000. Fibroblast growth factor 2: Its structure and property, paracrine function, tumor angiogenesis, and prostate-related mitogenic and oncogenic functions. Urology 55:800–806.

Giri D, Ropiquet F, Ittmann M. 1999. Alterations in expression of basic fibroblast growth factor (FGF) 2 and its receptor FGFR-1 in human prostate cancer. Clin Cancer Res 5:1063–1071.

Gross JL, Herblin WF, Dusak BA, Czerniak P, Diamond MD, Sun T, Eidsvoog K, Dexter DL, Yayon A. 1993. Effects of modulation of basic fibroblast growth factor on tumor growth in vivo. J Natl Cancer Inst 85:121–131.

Habeeb AF. 1966. Determination of free amino groups in proteins by trinitrobenzenesulfonic acid. Anal Biochem 14:328–336.

Halaban R, Ghosh S, Baird A. 1987. bFGF is the putative natural growth factor for human melanocytes. In Vitro Cell Dev Biol 23:47–52.

Halaban R, Kwon BS, Ghosh S, Delli Bovi P, Baird A. 1988. bFGF as an autocrine growth factor for human melanomas. Oncogene Res 3:177–186.

Hashida M, Kawakami S, Yamashita F. 2005. Lipid carrier systems for targeted drug and gene delivery. Chem Pharm Bull 53:871–880.

Hoganson DK, Chandler LA, Fleurbaaij GA, Ying W, Black ME, Doukas J, Pierce GF, Baird A, Sosnowski BA. 1998. Targeted delivery of DNA encoding cytotoxic proteins through high-affinity fibroblast growth factor receptors. Hum Gene Ther 9:2565–2575.

Hoganson DK, Sosnowski BA, Pierce GF, Doukas J. 2001. Uptake of adenoviral vectors via fibroblast growth factor receptors involves intracellular pathways that differ from the targeting ligand. Mol Ther 3:105–112.

Kawakami S, Wong J, Sato A, Hattori Y, Yamashita F, Hashida M. 2000. Biodistribution characteristics of mannosylated, fucosylated, and galactosylated liposomes in mice. Biochim Biophys Acta 1524:258–265.

Kawakami S, Munakata C, Fumoto S, Yamashita F, Hashida M. 2001. Novel galactosylated liposomes for hepatocyte-selective targeting of lipophilic drugs. J Pharm Sci 90:105–113.

Klagsbrun M, Sasse J, Sullivan R, Smith JA. 1986. Human tumor cells synthesize an endothelial cell growth factor that is structurally related to basic fibroblast growth factor. Proc Natl Acad Sci USA 83:2448–2452.

Klagsbrun M. 1989. The fibroblast growth factor family: Structural and biological properties. Prog Growth Factor Res 1:207–235.

Kleeff J, Fukahi K, Lopez ME, Friess H, Buchler MW, Sosnowski BA, Korc M. 2002. Targeting of suicide gene delivery in pancreatic cancer cells via FGF receptors. Cancer Gene Ther 9:522–532.

Kwabi-Addo B, Ozen M, Ittmann M. 2004. The role of fibroblast growth factors and their receptors in prostate cancer. Endocr Relat Cancer 11:709–724.

Lappi DA. 1995. Tumor targeting through fibroblast growth factor receptors. Semin Cancer Biol 6:279–288.

Managit C, Kawakami S, Yamashita F, Hashida M. 2005a. Effect of galactose density on asialoglycoprotein receptor-mediated uptake of galactosylated liposomes. J Pharm Sci 94:2266–2275.

Managit C, Kawakami S, Yamashita F, Hashida M. 2005b. Uptake characteristics of galactosylated emulsion by HepG2 hepatoma cells. Int J Pharm 301:255–261.

Maruyama K. 2002. PEG-immunoliposome. Biosci Rep 22:251–266.

Monsigny M, Roche AC, Midoux P. 1984. Uptake of neoglycoproteins via membrane lectin(s) of L1210 cells evidenced by quantitative flow cytofluorometry and drug targeting. Biol Cell 51:187–196.

Mosmann T. 1983. Rapid colorimetric assay for cellular growth and survival: Application to proliferation and cytotoxicity assays. J Immunol Methods 65:55–63.

Olsnes S, Klingenberg O, Wiedlocha A. 2003. Transport of exogenous growth factors and cytokines to the cytosol and to the nucleus. Physiol Rev 83:163–182.

Opanasopit P, Higuchi Y, Kawakami S, Yamashita F, Nishikawa M, Hashida M. 2001. Involvement of serum mannan binding proteins and mannose reseptors in uptake of mannosylated liposomes by macrophages. Biochim Biophys Acta 1511:134–145.

Penault-Llorca F, Bertucci F, Adelaide J, Parc P, Coulier F, Jacquemier J, Birnbaum D, deLapeyriere O. 1995. Expression of FGF and FGF receptor genes in human breast cancer. Int J Cancer 61:170–176.

Qin M, Escuadro B, Sharma S, Batra RK. 2005. Gene transfer mediated by native versus fibroblast growth factor-retargeted adenoviral vectors into lung cancer cells. Am J Respir Cell Mol Biol 32:211–217.

Rusnati M, Urbinati C, Tanghetti E, Dell'Era P, Lortat-Jacob H, Presta M. 2002. Cell membrane GM1 ganglioside is a functional coreceptor for fibroblast growth factor 2. Proc Natl Acad Sci USA 99:4367–4372.

Safran M, Eisenstein M, Aviezer D, Yayon A. 2000. Oligomerization reduces heparin affinity but enhances receptor binding of fibroblast growth factor 2. Biochem J 345:107–113.

Sapra P, Allen TM. 2003. Ligand-targeted liposomal anticancer drugs. Prog Lipid Res 42:439–462.

Schubert F, Zettl H, Hafner W, Krauss G, Krausch G. 2003. Comparative thermodynamic analysis of DNA–protein interactions using surface plasmon resonance and fluorescence correlation spectroscopy. Biochemistry 42:10288–10294.

Sosnowski BA, Gonzalez AM, Chandler LA, Buechler YJ, Pierce GF, Baird A. 1996. Targeting DNA to cells with basic fibroblast growth factor (FGF2). J Biol Chem 271:33647–33653.

Soulet F, Bailly K, Roga S, Lavigne AC, Amalric F, Bouche G. 2005. Exogenously added fibroblast growth factor 2 (FGF-2) to NIH3T3 cells interacts with nuclear ribosomal S6 kinase 2 (RSK2) in a cell cycle-dependent manner. J Biol Chem 280:25604–25610.

Stenlund P, Babcock GJ, Sodroski J, Myszka DG. 2003. Capture and reconstitution of G protein-coupled receptors on a biosensor surface. Anal Biochem 316:243–250.

Takanami I, Tanaka F, Hashizume T, Kikuchi K, Yamamoto Y, Yamamoto T, Kodaira S. 1996. The basic fibroblast growth factor and its receptor in pulmonary adenocarcinomas: An investigation of their expression as prognostic markers. Eur J Cancer 32:1504–1509.

Venkataraman G, Sasisekharan V, Herr AB, Ornitz DM, Waksman G, Cooney CL, Langer R, Sasisekharan R. 1996. Preferential self-association of basic fibroblast growth factor is stabilized by heparin during receptor dimerization and activation. Proc Natl Acad Sci USA 93:845–850.

Volm M, Koomagi R, Mattern J, Stammler G. 1997. Prognostic value of basic fibroblast growth factor and its receptor (FGFR-1) in patients with non-small cell lung carcinomas. Eur J Cancer 33:691–693.

Wegner GJ, Lee HJ, Marriott G, Corn RM. 2003. Fabrication of histidine-tagged fusion protein arrays for surface plasmon resonance imaging studies of protein–protein and protein–DNA interactions. Anal Chem 75:4740–4746.

Wu SJ, Chaiken I. 2004. Biosensor analysis of receptor-ligand interactions. Methods Mol Biol 249:93–110.

Yayon A, Aviezer D, Safran M, Gross JL, Heldman Y, Cabilly S, Givol D, Katchalski-Katzir E. 1993. Isolation of peptides that inhibit binding of basic fibroblast growth factor to its receptor from a random phage-epitope library. Proc Natl Acad Sci USA 90:10643–10647.

Ying W, Martineau D, Beitz J, Lappi DA, Baird A. 1994. Anti-B16-F10 melanoma activity of a basic fibroblast growth factor-saporin mitotoxin. Cancer 74:848–853.